HHS Public Access

Author manuscript

*Cell Rep*. Author manuscript; available in PMC 2023 January 13.

Published in final edited form as:

*Cell Rep*. 2022 December 13; 41(11): 111821. doi:10.1016/j.celrep.2022.111821.

# *AKTIP* loss is enriched in ERα-positive breast cancer for tumorigenesis and confers endocrine resistance

**Angel S.N. Ng**[1], **Shibo Zhang**[1,8], **Victor C.Y. Mak**[1,8], **Yuan Zhou**[1], **Yin Yuen**[1], **Rakesh Sharma**[2], **Yiling Lu**[3], **Guanglei Zhuang**[4,5], **Wei Zhao**[6], **Herbert H. Pang**[7], **Lydia W.T. Cheung**[1,9,*]

[1]School of Biomedical Sciences, Li Ka Shing Faculty of Medicine, The University of Hong Kong, Hong Kong, China

[2]Proteomics and Metabolomics Core, Center for PanorOmic Sciences, Li Ka Shing Faculty of Medicine, The University of Hong Kong, Hong Kong, China

[3]Department of Genomic Medicine, Division of Cancer Medicine, UT MD Anderson Cancer Center, Houston, TX 77030, USA

[4]State Key Laboratory of Oncogenes and Related Genes, Department of Obstetrics and Gynecology, Shanghai Cancer Institute, Ren Ji Hospital, Shanghai Jiao Tong University School of Medicine, Shanghai 200240, China

[5]Shanghai Key Laboratory of Gynecologic Oncology, Ren Ji Hospital, Shanghai Jiao Tong University School of Medicine, Shanghai 200240, China

[6]Integrative Tumor Epidemiology Branch, Division of Cancer Epidemiology and Genetics, National Cancer Institute, National Institutes of Health, Department of Health and Human Services, Bethesda, MD 20892, USA

[7]School of Public Health, Li Ka Shing Faculty of Medicine, The University of Hong Kong, Hong Kong, China

[8]These authors contributed equally

[9]Lead contact

## SUMMARY

Recurrent deletion of 16q12.2 is observed in luminal breast cancer, yet the causal genomic alterations in this region are largely unknown. In this study, we identify that loss of *AKTIP*, which is located on 16q12.2, drives tumorigenesis of estrogen receptor alpha (ERα)-positive, but



*Correspondence: lydiacwt@hku.hk.

AUTHOR CONTRIBUTIONS

L.W.T.C. conceived and coordinated the project. L.W.T.C. designed the experiments. A.S.N.N., S.Z., V.C.Y.M., Y.Z., and Y.Y. performed experiments. R.S. contributed to mass spectrometry analysis. Y.L. contributed to RPPA experiments. A.S.N.N., V.C.Y.M., S.Z., G.Z., W.Z., H.H.P., and L.W.T.C. analyzed the data. L.W.T.C. wrote the manuscript with input from the other authors.

DECLARATION OF INTERESTS

The authors declare no competing interests.

SUPPLEMENTAL INFORMATION

Supplemental information can be found online at https://doi.org/10.1016/j.celrep.2022.111821.

not ERα-negative, breast cancer cells and is associated with poor prognosis of patients with ERα-positive breast cancer. Intriguingly, *AKTIP*-depleted tumors have increased ERα protein level and activity. Cullin-associated and neddylation-dissociated protein 1 (CAND1), which regulates the cullin-RING E3 ubiquitin ligases, protects ERα from cullin 2-dependent proteasomal degradation. Apart from ERα signaling, *AKTIP* loss triggers JAK2-STAT3 activation, which provides an alternative survival signal when ERα is inhibited. *AKTIP*-depleted MCF7 cells and ERα-positive patient-derived organoids are more resistant to ERα antagonists. Importantly, the resistance can be overcome by co-inhibition of JAK2/STAT3. Together, our results highlight the subtype-specific functional consequences of *AKTIP* loss and provide a mechanistic explanation for the enriched *AKTIP* copy-number loss in ERα-positive breast cancer.

## Graphical Abstract

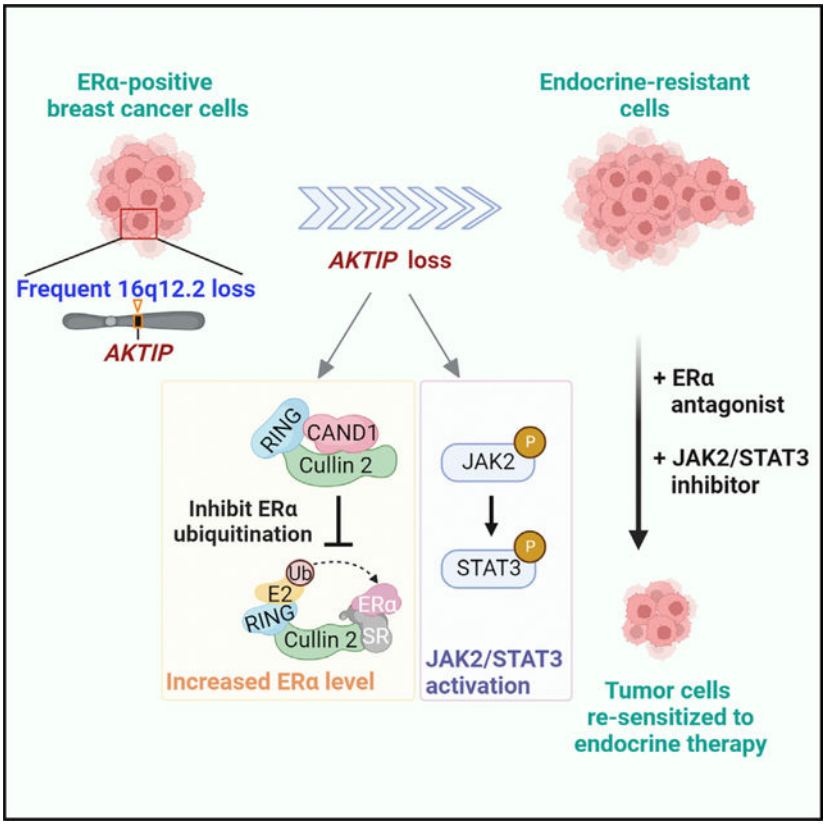


## In brief

Ng et al. report *AKTIP* loss at 16q12.2 as a functional aberration of ERα-positive breast cancer and the therapeutic approach to target such aberration. They show that ERα stabilization and JAK2/STAT3 activation are the mechanisms underlying the enhanced tumorigenesis and endocrine resistance.

## INTRODUCTION

Breast cancer is partitioned based on the mRNA expression of 50 genes (PAM50) into 5 intrinsic molecular subtypes, including luminal A, luminal B, basal (triple-negative), human epidermal growth factor receptor 2 (HER2)-enriched, and normal-like.[1,2] These subtypes have unique histopathological features, clinical manifestations, and responses to systemic therapies. Apart from distinct gene expression patterns, genomic profiling of breast cancer samples has revealed somatic aberration patterns that are enriched in particular molecular subtypes of the disease.[3,4] For example, highly frequent focal loss of 16q12.2 in luminal or estrogen receptor alpha (ERα)-positive breast tumors has been reported in several independent cohorts.[4–7] Within this locus, *RBL2* is a relatively well-established tumor suppressor that inhibits E2F-dependent transcription and cell-cycle progression in multiple cancer types, including breast cancer,[8,9] whereas *RPGRIP1L* is a potential tumor suppressor as demonstrated in hepatocellular carcinoma cell lines.[10]

The luminal A and luminal B subtypes, which account for 60%–70% of breast cancers, are distinct from the other subtypes by being ERα-positive. Luminal B tumors tend to be more aggressive and are associated with worse prognosis than luminal A tumors.[11,12] The standard treatments for luminal tumors are endocrine therapy (e.g., tamoxifen) and chemotherapy. However, around 1/3 of the patients who initially respond to tamoxifen would eventually relapse with endocrine-resistant disease.[13] Endocrine resistance can be driven by *ESR1* mutation,[14,15] loss of ERα expression,[16] or aberrant expression of ERα co-regulators that modulate ERα-mediated transcription.[17,18] Additional resistance mechanism includes activation of receptor tyrosine kinases and the downstream AKT or MAPK pathway, which in turn limits the cytotoxicity of the ERα inhibitor by providing a bypass survival signal or by inducing ligand-independent ERα activation.[19–22] Recent studies have also demonstrated that altered DNA methylation or mutation at ERα-binding sites causes reprogramming of ERα cistrome and endocrine resistance.[23,24]

Here, we show that loss of *AKTIP* on 16q12.2 is a prognostically and therapeutically relevant chromosomal aberration in ERα-positive breast cancer. *AKTIP*-depleted ERα-positive breast tumor cells are tumorigenic and resistant to ERα antagonists. The subtype-specific effects of *AKTIP* loss in ERα-positive tumors suggest that the aberration is recurrent in this particular subtype for functional advantages.

## RESULTS

### *AKTIP* loss promotes tumorigenic phenotypes selectively in luminal breast cancer cells

Homozygous and heterozygous loss of *AKTIP* were detected in 1.5% and 54.5% of The Cancer Genome Atlas (TCGA) breast cancer cases, respectively (Figure S1A). There was a significant association between *AKTIP* copy number and breast cancer subtypes (Kruskal-Wallis test; $p = 0.007$), with luminal tumors displaying a higher proportion of *AKTIP* loss than the other subtypes (Figure S1B). Indeed, *AKTIP* copy numbers were significantly lower in luminal tumors or ERα-positive tumors than tumors of the other subtypes or ERα-negative tumors (Figure S1C). The copy number of *AKTIP* correlates with its mRNA levels ($r = 0.69$, $p < 0.0001$; Figure S1D), suggesting a possible causal relationship. Importantly,

*AKTIP* mRNA levels were significantly lower in breast tumors compared with their matched normal breast tissues ($p < 0.0001$, Wilcoxon signed-rank test; Figure 1A).

We then evaluated the association between *AKTIP* mRNA levels and patient survival outcomes using a Kaplan-Meier (KM) plotter and METABRIC dataset.[25,26] Intriguingly, low *AKTIP* mRNA levels were associated with poor survival in patients with ERα-positive breast cancer in the KM plotter dataset (patients divided at lower tertile: hazard ratio [HR] = 1.27, 95% confidence interval [CI] = 1.04–1.54, p = 0.017; not significant for patients divided at median or quartile) and in METABRIC dataset (divided at median: HR = 1.15, 95% CI = 1.01–1.32, p = 0.037; or lower tertile: HR = 1.16, 95% CI = 1.01–1.35, p = 0.036; Figures 1B and S2A; Table S1). No association was observed in patients who were ERα-negative or that were stratified based on the status of progesterone receptor or HER2 in both datasets (Figures 1B and S2A; Table S1). When patients in these two datasets were stratified into the intrinsic molecular subtypes, a significant association between low *AKTIP* mRNA levels and poor survival was observed in patients with luminal B (KM plotter samples divided at lower tertile: HR = 1.47, 95% CI = 1.08–2.00, p = 0.016; METABRIC samples divided at median: HR = 1.48, 95% CI = 1.20–1.88, p = 0.0005; Figures S2B and S2C), suggesting that the shorter survival in patients who were ERα-positive might be mainly attributed to the luminal B subpopulation. Further, analysis of TCGA breast cancer data identified that *AKTIP* gene copy loss was associated with a trend (although not statistically significant) toward shorter progression-free survival in patients with luminal A or luminal B (Figure S2D) and a significantly shorter survival in patients with luminal B in METABRIC cohort (HR = 1.27, 95% CI = 1.01–1.60, p = 0.043; Figure S2E). No trend was noted in patients of basal, HER2-enriched, or normal-like subtype (Figures S2D and S2E). These findings together suggested that copy-number loss of *AKTIP* is enriched in the ERα-positive tumors and that *AKTIP* depletion correlates with poor patient survival, particularly in the luminal B subtype. We therefore hypothesized that *AKTIP* may be selectively deleted in ERα-positive breast cancer for functional advantages.

To explore this possibility, we investigated the functional consequences of *AKTIP* loss using siRNA knockdown in breast cancer cell lines of different subtypes. The efficiency of the siRNA was presented in Figures S3A–S3C. Depletion of *AKTIP* enhanced viability consistently in 5 ERα-positive breast cancer cell lines, MCF7, MDA-MB-361, MDA-MB-175, BT474, and T47D (Figures 1C and S3D). On the contrary, *AKTIP* depletion had no effect on the viability of HER2-enriched cell lines (SKBR3 and HCC1954) and basal cell lines (MDA-MB-231 and MDA-MB-468) (Figure 1C) despite efficient knockdown of *AKTIP*. In addition, cell migration and invasion capabilities were enhanced upon *AKTIP* loss in MCF7 and MDA-MB-361 (Figure 1D) but not in HER2-enriched or basal cells (Figures 1D and S3E).

The functional impacts of *AKTIP* loss were further examined in MCF7 cells with stable *AKTIP* knockdown (Figure S4A). Consistently, increases in viability, long-term clonogenic growth, migration, and invasion could be observed in these cells compared with empty-vector-expressing or parental cells (Figures S4B–S4D). The stable cells were injected subcutaneously into female nude mice (n = 10). Tumors were collected 6 weeks post-

injection. The weight and volume of the *AKTIP*-depleted tumors were both higher than that of the vector tumors (Figures 1E and S4E).

## *AKTIP* loss leads to increased ERα protein levels in luminal breast cancer cells

We investigated the downstream signaling that is induced in cells with *AKTIP* loss. Reverse-phase protein array (RPPA) was performed using *AKTIP* small interfering RNA (siRNA)- or mock-transfected MCF7 cells. Proteins with changes in expression levels >20% upon *AKTIP* loss are shown in a heatmap (Figure 2A). Surprisingly, in contrast to the previous reported roles as a binding partner of AKT and an inducer of AKT phosphorylation in HEK293 and Jurkat cells,[27] knockdown of *AKTIP* had no impact on the phosphorylation of AKT pathway components including AKT, mTOR, p70S6K, and S6 (Figure 2A). Western blotting with MCF7 and MDA-MB-361 cells confirmed these results (Figure 2B). Binding between AKTIP and AKT was not detected by immunoprecipitation experiments, in which we included a positive control HOOK1, which has been reported to bind AKTIP[28] (Figure S5A). This was also observed in another study, which could not identify an interaction between AKTIP and AKT.[28] Moreover, the lack of effect of AKTIP on AKT signaling was observed in HER2-overexpressing SKBR3 cells (Figure S5B).

Other remarkable findings are increases in total ERα and phosphorylated ERα (S118) proteins in *AKTIP*-depleted MCF7 cells (Figure 2A). S118 is a well-characterized phosphorylation site in stimulating ERα transcriptional activity.[29] These increases were validated by western blotting in MCF7 and MDA-MB-361 (Figure 2C). In addition to S118 phosphorylation, we observed increased levels of phosphorylated ERα at S167 and S104/106, which are the other phosphorylation sites involved in transcriptional activation of ERα.[29] As S118, S167, and S104/106 are phosphorylated by different kinases and can be phosphorylated independent of each other,[30] it is likely that the increased ERα phosphorylation upon *AKTIP* loss is a result of total ERα protein upregulation. Co-expression of the *AKTIP* open reading frame could rescue the increased ERα level caused by siRNA targeting the 3′ UTR of *AKTIP*, demonstrating the specificity (Figure 2D). Immunohistochemical staining of xenograft tumors presented in Figure 1E showed that *AKTIP*-depleted tumors had higher levels of ERα and cell proliferation marker Ki67 (Figure 2E). The association between *AKTIP* and total ERα protein levels was further examined in ERα-positive breast cancer patient samples (n = 65). Consistently, an inverse correlation between ERα and *AKTIP* levels was observed ($r = -0.25$; $p < 0.05$; Figure 2F), further supporting the upregulation of ERα in *AKTIP*-low breast tumors. ERβ has been demonstrated to counteract the proliferative effects driven by ERα.[31] We therefore examined ERβ levels upon *AKTIP* knockdown. It was found that *AKTIP* knockdown did not alter ERβ protein levels in the ERα-positive breast cancer cells (Figure 2G).

## Protein stability of ERα is enhanced in cells with *AKTIP* loss

We then attempted to understand the mechanisms underlying the increase in total ERα protein level observed upon *AKTIP* loss. Real-time PCR revealed no significant difference in ESR1 mRNA levels upon *AKTIP* knockdown in MCF7 and MDA-MB-361 cells (Figure S5C), demonstrating that transcriptional regulation unlikely contributes to the increased ERα protein level. ERα protein turnover was assessed by cycloheximide chase experiment.

Strikingly, ERα protein in *AKTIP* knockdown cells degraded less rapidly compared with vector control cells (Figure 3A). Increased protein stability of ERα was further supported by a decrease in ERα poly-ubiquitination after *AKTIP* knockdown in MCF7 and MDA-MB-361 cells (Figures 3B and S5D).

AKTIP is a ubiquitin E2 variant (UEV) that contains an inactive E2 ubiquitin-conjugating domain due to the lack of a catalytic cysteine residue.[32] Although UEVs may not bind to ubiquitin, UEVs characterized previously have demonstrated the ability to indirectly regulate proteasomal degradation by regulating the expression or the activity of the other ubiquitin-proteasome pathway members.[33,34] Intriguingly, mass-spectrometry-based protein interactome profiling and STRING analysis[35] revealed a network of 23 AKTIP-bound proteins with potential roles in the post-translation regulation of ERα expression, as demonstrated in the literature (Figure 3C). siRNA (pool of 4 siRNA per gene) of 7 genes that are known to inhibit the ubiquitination pathway was transfected into *AKTIP*-depleted cells. Depletion of cullin-associated and neddylation-dissociated protein 1 (CAND1), which was validated to bind AKTIP (Figure S5E), led to a reduction of ERα protein levels in *AKTIP*-depleted cells (Figure 3D). The other 6 genes had no effect. AKTIP has been shown to form complex with the Hook family of coiled-coil proteins (HOOK1, HOOK2, and HOOK3) to promote protein trafficking.[28] Our data showed that the Hook proteins were not involved in ERα stabilization by AKTIP (Figure S5F). We confirmed the findings using individual siRNAs. Consistently, *CAND1* siRNA reduced ERα protein levels in MCF7 and MDA-MB-361 cells (Figures 3E and S5G), with an increase in ERα ubiquitination (Figure 3F). siRNA of *USP7* and *FASN*, which have been previously shown to regulate ERα,[36,37] had no significant effect on *AKTIP* loss-induced ERα levels (Figure S5H). These data suggested that CAND1 mediates ERα protein stabilization.

CAND1 physically interacts with the cullin family proteins.[38] Cullin serves as a scaffold of the multiprotein cullin-RING E3 ubiquitin ligase (CRL) complex that mediates covalent attachment of ubiquitin to substrates.[39] It has been suggested that CAND1-bound CRL is inactive, whereas conjugation of ubiquitin-like protein NEDD8 (neddylation) to cullin activates CRL.[38,40,41] It is noteworthy that NEDD8 has been shown to cause ERα ubiquitination and degradation.[42] Further, one of the cullin members, cullin 2 (CUL2), was identified in our AKTIP interactome analysis (Figure 3C). These results together led us to investigate the possibility that the effect of CAND1 on ERα protein degradation is manifested through CUL2. First, overexpression of CUL2 or NEDD8 abolished the upregulated ERα protein levels in *AKTIP*-depleted cells (Figure 3G). Next, the binding between CUL2 and CAND1 was enhanced in *AKTIP*-depleted cells (Figure 3H). In contrast, the binding between CUL2 and ERα was markedly reduced upon *AKTIP* loss (Figure 3I). Binding between ERα and CAND1 could not be detected, whereas binding between ERα and a known protein binding partner HSP70[43] was observed in the same experiment (Figure S5I).

### MCF7 cells with *AKTIP* loss exhibit ERα-responsive gene expression profiles

ERα in the nucleus binds to estrogen response element (ERE) to regulate transcription of target genes. The transcriptional activity of ERα can be modulated through ERα

phosphorylation.[44] We therefore investigated whether the increased ERα expression and phosphorylation is translated to its function as a transcription factor in *AKTIP*-depleted cells. A subcellular fractionation experiment revealed that the upregulated total ERα and ERα pS118 proteins primarily accumulated in the nucleus upon *AKTIP* loss (Figure 4A). Luciferase assay using a firefly luciferase reporter linked to three copies of ERE (3X-ERE-TATA) demonstrated concomitant increase in the transcriptional activity of ERα (Figure 4B).

To examine the transcriptome changes upon *AKTIP* depletion, RNA sequencing (RNA-seq) analysis was performed using *AKTIP* siRNA-transfected and mock-transfected cells. Intriguingly, there were 91 differentially expressed genes (DEGs) upon *AKTIP* knockdown (adjusted $p < 5\%$, fold change > 1.2) in MCF7 cells, whereas only 17 genes were altered in the ERα-negative SKBR3 cells (Figures 4C and 4D). Remarkably, 89% of the 91 DEGs identified in MCF7 were defined as estrogen-responsive genes based on the transcriptomic data in the Signaling Pathways Project[45,46] (Figure 4E; Table S2). The DEGs were further subjected to gene set enrichment analysis,[47] which showed significant enrichment in early and late estrogen response hallmark gene sets (Figure 4F). We validated 12 DEGs with high or low fold change and documented functional roles in cancers by real-time PCR (Figure S6A). Notably, the expression levels of classical ERα targets (*TFF1*, *GREB1*, *CCND1*) were increased in MCF7 and MDA-MB-361 cells but not in SKBR3 after *AKTIP* knockdown (Figures 4G and S6A). Therefore, it is reasonable to speculate that the fewer alterations observed in the transcriptome of SKBR3 compared with MCF7 upon *AKTIP* loss was due to the absence of ERα. The mRNA levels of *AKTIP* in MCF7 and MDA-MB-361 cells were not altered upon β-estradiol stimulation, suggesting that *AKTIP* is not a transcriptional target of ERα and that there is no feedback from ERα to AKTIP (Figure S6B).

SGK3 is a downstream transcriptional target of ERα[48] and can sustain ERα signaling.[49] Increased *SGK3* mRNA levels were evident in RNA-seq and real-time PCR validation in *AKTIP*-depleted MCF7 and MDA-MB-361 cells (Figure 4G). This upregulation of *SGK3* was abolished in the presence of the ERα antagonist fulvestrant (Figure 4H), indicating that the upregulation was mediated through ERα. Similarly, loss of *AKTIP* increased the protein levels of SGK3 and its phosphorylation at T320 in both MCF7 and MDA-MB-361 cells (Figure 4I), whereas inhibition of ERα by fulvestrant or tamoxifen (4-OH-Tam) abrogated the increases (Figure S6C). Concordant with these findings that SGK3 upregulation is mediated through ERα, *AKTIP* loss had no effect on total SGK3 and phosphorylated SGK3 proteins in ERα-negative cell lines SKBR3 and MDA-MB-453 (Figure 4I). We next examined whether the upregulation of SGK3 plays a role in sustaining ERα activation. siRNA-mediated knockdown of *SGK3* did not alter the extent of ERα upregulation upon *AKTIP* loss (Figure S6D). Together, the above data suggest that while SGK3 is upregulated through transcriptional activation of ERα, SGK3 does not sustain ERα activation in *AKTIP*-depleted cells.

## Loss of *AKTIP* activates JAK2/STAT3 signaling in ERα-positive breast cancer cells

The data have established positive regulation of ERα in *AKTIP*-depleted cells; we therefore examined the consequences of silencing ERα on cell viability. Results showed that

the viability of cells with *ESR1* knockdown was inhibited compared with that of mock-transfected cells (Figure 5A). Yet, cells with *AKTIP* loss still exhibited stronger viability than vector control cells in spite of the comparable knockdown efficiency (Figure 5A). This observation implicated the presence of an additional survival signal that the cells can rely on despite ERα signaling being inhibited.

Interestingly, RPPA data revealed an increase in JAK2 level upon *AKTIP* loss in MCF7 cells (Figure 2A). We validated this change by western blotting and explored the potential effects of *AKTIP* loss on the activation of JAK2 and its downstream molecule STAT3. Phosphorylated STAT3 at Y705 and phosphorylated JAK2 at Y1007/1008 were enhanced in two *AKTIP*-depleted ERα-positive cell lines MCF7 and MDA-MB-361 (Figure 5B), demonstrating an activation of the JAK2/STAT3 signaling pathway. There was no significant change in the levels of total STAT3 or JAK2. The activation of JAK2/STAT3 signaling was specific to ERα-positive breast cancer cells because knockdown of *AKTIP* had no significant impact on the pathway in the ERα-negative SKBR3 and MDA-MB-453 (Figure 5B).

The potential crosstalk between the activated ERα and JAK2/STAT3 signaling cascades was assessed. The increases in phosphorylated STAT3 and JAK2 levels upon *AKTIP* loss were not altered by the ERα antagonists (fulvestrant and 4-OH-Tam) (Figure 5C) or knockdown of *SGK3* (Figure 5D). STAT3 inhibition either by treatment with JAK2 inhibitor AZD1480, *STAT3* siRNA, or STAT3 inhibitor BBI608 in *AKTIP*-depleted cells did not attenuate the activation of ERα and SGK3 (Figures 5E and 5F). These data indicate that ERα and JAK2/STAT3 signaling are activated independently upon *AKTIP* loss.

## *AKTIP* loss renders cells resistant to ERα antagonists and JAK2 inhibition overcomes the resistance

We investigated the drug responses of *AKTIP*-depleted cells toward ERα or JAK2/STAT3 inhibition. *AKTIP*-depleted MCF7 or MDA-MB-361 cells were more resistant to fulvestrant or 4-OH-Tam compared with vector control cells (Figures 6A and S7A). The efficiency of fulvestrant in downregulating ERα protein was validated by western blotting (Figure 6A, right panel). Interestingly, among the group of patients with ERα-positive breast cancer who received adjuvant tamoxifen therapy, patients with low *AKTIP* mRNA levels had a higher risk of developing recurrence, further supporting that *AKTIP*-low tumors may be endocrine resistant (Figure 6B). *AKTIP*-depleted MCF7 or MDA-MB-361 cells also displayed resistance toward JAK2 inhibition when cells were treated with AZD1480 alone (Figures 6C and S7A). The resistance to ERα antagonists or JAK2 inhibitor might be explained by the notion that *AKTIP*-depleted cells are driven by these two independent signaling pathways and that single pathway inhibition is insufficient to cause cell death.

We thus examined whether inhibition of JAK2 could modulate the response of *AKTIP*-depleted cells to ERα antagonists. Remarkably, the addition of a fixed concentration of JAK2 inhibitor AZD1480 increased the sensitivity of *AKTIP*-depleted MCF7 or MDA-MB-361 cells to fulvestrant or 4-OH-Tam (Figures 6D and S7B), demonstrating that JAK2/STAT3 inhibition can resensitize *AKTIP*-depleted cells to ERα inhibition. AZD1480 had no effect on the dose-response curve of fulvestrant or 4-OH-Tam in vector control or

mock-transfected cells (Figures 6D and S7B). Similar observations were obtained when cells were treated with STAT3 inhibitor C188–9 (Figures 6E and S7C).

In mice bearing *AKTIP*-depleted MCF7 tumor cells, we showed that AZD1480 and 4-OH-TAM combination resulted in marked suppression of tumor growth, whereas single treatment with either inhibitor did not have any pronounced effect (Figure 7A). We further extended our observations using human ERα-positive breast cancer organoid models. Consistent with the observations in cell lines, we verified that *AKTIP* loss led to increased ERα protein level and cell viability (Figures 7B and 7C). Strikingly, we also found that the organoids were more resistant to 4-OH-Tam upon *AKTIP* depletion and that JAK2 inhibitor AZD1480 or STAT3 inhibitor BBI608 resensitized the cells to 4-OH-Tam (Figure 7D).

## DISCUSSION

The *AKTIP* gene is aberrated in multiple cancer types from TCGA.[50] *AKTIP* deletion (heterozygous and homozygous) is predominant over amplification and is most frequent in ovarian and breast cancers, whereas endometrial and stomach cancers are the cancer lineages with the most frequent *AKTIP* small-nucleotide mutations. Available data so far have demonstrated both oncogenic and tumor-suppressive properties of *AKTIP* depending on the cell types. We have previously reported that *AKTIP* inhibited the viability of an interleukin-3-dependent non-tumorigenic cell line and endometrial cancer cell lines.[51] In contrast, *AKTIP* appears to be an oncogene in cervical cancer. *AKTIP* expression enhanced cell migration, and *AKTIP* knockdown led to cell-cycle arrest and apoptosis.[52,53] Interestingly, copy-number alteration of *AKTIP* does not correlate with its oncogenic role in cervical cancer, which has more frequent copy-number loss than copy-number gain. The other reported regulatory mechanisms of *AKTIP* expression include transcriptional regulation by p53 or post-transcriptional regulation by miRNA.[54,55]

ERα can be mono-ubiquitinated or poly-ubiquitinated. ERα mono-ubiquitination, for example by E3 ubiquitin ligases RNF31 and RNF8, promotes ERα stabilization.[56,57] ERα poly-ubiquitination triggers proteasomal degradation and can be mediated by different RING E3 ligases (CHIP, Mdm2, BRCA1, Skp2),[58–61] HECT E3 ligase E6AP,[62] and atypical E3 ligase Hbo1.[63] The multi-unit CRL is composed of cullin (as scaffold), RING finger protein RBX1/2 (for binding to E2 ubiquitin-conjugating enzyme), and a specific set of substrate receptors that recognize the ubiquitination target.[39,64] CAND1 has been shown to cause dissociation of substrate receptor from cullin and inhibit CRL activity.[38,40,65] Later studies also showed that CAND1 controls the composition of substrate receptor subunits in CRL.[66,67] Among the 8 cullin protein members, CUL3-RING ligase with the substrate adaptor SPOP and CUL7 coupled with substrate adaptor Skp2 have been reported to mediate ERα poly-ubiquitination.[61,68] In this study, we demonstrated a role of CUL2 in ERα regulation. The reduced ERα ubiquitination in *AKTIP*-depleted cells could be due to (1) decreased binding of ERα to CUL2 and (2) inhibited CUL2 activity by enhanced CAND1-CUL2 binding (Figure 7E). The mechanism underpinning these altered protein interactions remains to be elucidated.

AKTIP may contribute to different steps along the protein degradation pathway through participating in different protein complexes. In addition to a potential role in regulating E3 ligase as demonstrated in this study, accumulating evidence has indicated that AKTIP is involved in endosomal trafficking, during which ubiquitinated cargos are sorted into the endolysosomal pathway. AKTIP is part of a HOOK protein-containing protein complex that interacts with the homotypic vesicular protein sorting (HOPS) complex.[28] AKTIP promotes late endosome/lysosome clustering and fusion mediated by HOPS.[28,69] The regulation of ERα by AKTIP is probably not mediated through this complex because silencing the HOOK proteins had no effect on the regulation. It has also been shown that the UEV domain of AKTIP binds to a functional complex in vesicle biogenesis called endosomal sorting complex required for transport (ESCRT).[70,71] The functional role of the UEV domain in post-translational regulation of proteins warrants further investigation.

JAK2/STAT3 signaling promotes cell proliferation and progression of ERα-positive or ERα-negativebreastcancer.[72–74]Crosstalk between STAT3 and ERα signaling is context dependent. While β-estradiol inhibited interleukin-6-induced STAT3 activity,[75,76] ERα enhanced STAT3 activity under leptin stimulation.[77] Similarly, negative and positive regulation of ERα signaling by JAK2 has been demonstrated.[78,79] Our data suggested the activation of JAK2/STAT3 signaling as an alternative ERα-independent pathway for *AKTIP*-depleted cells to escape ERα inhibition. Similar to our observations, a previous study has reported JAK2/STAT3 activation in tamoxifen-resistant MCF7 cells.[80] Inhibition of JAK2/STAT3 by chemical inhibitor or gene silencing increased tamoxifen sensitivity.[80] A recent phase II study of a JAK1/2 inhibitor (ruxolitinib) combined with a steroidal aromatase inhibitor (AI) in patients with non-steroidal-AI-resistant ERα+ breast cancer showed that 24% of the treated patients (6/25) achieved stable disease.[81] The incorporation of predictive biomarkers may further increase treatment efficacy.

In summary, our results have revealed the prognostic and therapeutic values of *AKTIP* loss in ERα-positive breast cancer. Copy-number loss of *AKTIP* may serve as a biomarker for predicting endocrine resistance and sensitivity toward treatment regimens co-targeting ERα and JAK2/STAT3 signaling.

## Limitations of the study

Our proposal that *AKTIP* depletion leads to reduced activity of CUL2-containing ligase through altered binding to CAND1 needs to be validated. Future studies are warranted to better understand the binding between AKTIP, CAND1, and CUL2 as well as the functional impact of such binding. So far, reported data on the regulation of CAND1-cullin binding are conflicting. Neddylation of cullin or expression of substrate receptor led to dissociation of cullin from CAND1 in HeLa or HEK293T cells.[40,82] However, in another study, inhibiting neddylation or knockdown of substrate receptor did not increase CAND1 binding to cullin in HEK293.[83] Regardless, we did not observe any significant change in the levels of neddylated CUL2 in *AKTIP*-depleted cells (Figure 3G). Therefore, the enhanced CAND1-CUL2 interaction in the cells is unlikely to involve the neddylation-associated mechanism. Second, the mechanism of JAK2 activation in *AKTIP*-depleted cells remains

to be elucidated. A fuller understanding of the activation mechanism may yield additional insights into endocrine resistance.

## STAR★METHODS

Detailed methods are provided in the online version of this paper and include the following:

### RESOURCE AVAILABILITY

**Lead contact—**Further information and requests for resources and reagents should be directed to and will be fulfilled by the lead contact, Lydia W.T. Cheung (lydiacwt@hku.hk).

**Materials availability—**Plasmid generated in this study is available from the lead contact upon request.

#### Data and code availability

- The RNA-seq data have been deposited to the Gene Expression Omnibus (GEO). The IP-MS data have been deposited to the ProteomeXchange Consortium via the PRIDE. Accession numbers are listed in the key resources table.
- This paper analyzes existing, publicly available data. The TCGA breast cancer dataset was downloaded from the Broad GDAC Firehose (http://gdac.broadinstitute.org/). The METABRIC dataset was downloaded from cBioPortal (https://www.cbioportal.org/study/summary?id=brca_metabric).
- This paper does not report original code.
- Any additional information required to reanalyze the data reported in this paper is available from the lead contact upon request.

### EXPERIMENTAL MODEL AND SUBJECT DETAILS

**Cell lines—**MCF7, MDA-MB-361, MDA-MB-175, BT474, T47D, MDA-MB-453, SKBR3, MDA-MB-231, HCC1954 and MDA-MB-468 were obtained from American Type Culture Collection (Manassas, VA). Cells were maintained in RPMI1640 (Gibco, Carlsbad, CA) supplemented with 8% fetal bovine serum (FBS; Gibco),100 units/mL penicillin and 100 μg/mL streptomycin (Gibco) in a humidified environment at 37°C with constant supply of 5% $CO_2$. All cell lines were tested for mycoplasma contamination and validated by short tandem repeat profiling.

**Organoid—**Human breast cancer organoid PDM-195 (HCM-CSHL-0366-C50) was obtained from American Type Culture Collection. According to the data provided in the Human Cancer Models Initiative Searchable Catalog, this model is a primary tumor that is ERα-positive, PR-negative and HER2-negative as assessed by IHC. The organoid was maintained in polymerized droplets of Cultrex reduced growth factor basement membrane extract (BME) (type 2, Pathclear) (R&D systems, Minneapolis, MN) in advanced DMEM/F12 (Thermo Fisher Scientific, Waltham, MA) supplemented with B-27 supplement (Thermo Fisher Scientific), 2 nM L-glutamine (Thermo Fisher Scientific), 10 mM Nicotinamide (Sigma-Aldrich, St. Louis, MO), 1.25 mM N-acetylcysteine (Sigma-Aldrich),

100ng/mL Noggin (PeproTech, Rocky Hill, NJ), 5 ng/mL EGF (PeproTech), 20 ng/mL FGF-10 (PeproTech), 5 ng/mL FGF-7 (PeproTech), 5 nM Neuregulin-1 (PeproTech), 500 nM A83–01 (PeproTech), 250 ng/mL R-spondin-1 (PeproTech), 10 mM HEPES (Thermo Fisher Scientific), 1 μM SB202190 (LC Laboratories, Woburn, MA), 100 units/mL penicillin and 0.1 mg/mL streptomycin (Gibco). For passaging, collected organoids were dissociated using TrypLE Express (Thermo Fisher Scientific), pelleted and resuspended in ice-cold BME. BME-cell suspension in form of 10 μL droplets were allowed to solidify as domes on a prewarmed culture plate at 37°C before adding complete advanced DMEM/F12 culture medium supplemented with 10 μM ROCK inhibitor Y-27632 (LC Laboratories) for cell recovery. Organoids were grown for 10 to 14 days under a humidified atmosphere of 5% $CO_2$ at 37°C. Change of complete culture medium was performed every other day.

**Xenograft—**All animal procedures were approved by the Committee on the Use of Live Animals in Teaching and Research at the University of Hong Kong. Experiments were performed according to ethical regulations. Female BALB/cAnN-nu (nude) mice were obtained from the Charles River Lab (Stone Ridge, NY) and kept in the animal facility with a 12-hr light-dark cycle and *ad libitum* access to food and water. Six-week-old mice were used in this study.

## METHOD DETAILS

**siRNAs, plasmids and transfection—**ON-TARGETplus siRNA targeting human *AKTIP*, *SGK3* and *STAT3* as well as SMARTpool ON-TARGETplus siRNA targeting 10 AKTIP-bound proteins were purchased from Dharmacon (Lafayette, CO). *ESR1*, *CAND1*, *FASN* and *USP7* siRNA were obtained from Integrated DNA Technologies (Coraville, IA). The siRNA sequences are listed in Table S3. Lipofectamine RNAiMAX (Invitrogen, Carlsbad, CA) was used to transfect siRNA at 10 nM. shRNA against *AKTIP* in pLKO.1-Puro lentiviral vector was developed by The RNAi Consortium (TRC).[87] pcDNA3-myc3-CUL2 and pcDNA3-myc3-NEDD8 were gifts from Yue Xiong (Addgene plasmid # 19892 and # 19943).[84,85] Transfection of plasmids was performed using Lipofectamine 3000 (Invitrogen). MCF7 cells stably expressing *AKTIP* shRNA or vector control were established by lentiviral transduction followed by puromycin selection.

**Cell viability assay—**siRNA-transfected or stable cells were seeded into 96-well plates in triplicate at the density of 1,000 cells per well. At indicated time points, cells were incubated with 0.2 mg/mL resazurin (Sigma-Aldrich) for 4 hrs prior to measurement of absorbance at 600 nm.

**Migration and invasion assays—**siRNA-transfected or stable cells were suspended in serum-free medium and seeded into the upper chamber of cell culture inserts of 8 μm pore size (Millipore, Billerica, MA) with or without 1 mg/mL Matrigel coating (Corning, Glendale, AZ) for invasion and migration assays respectively. Cells were allowed to invade or migrate towards the lower chambers filled with medium containing 10% FBS for 16 hrs prior to fixing with methanol and staining with crystal violet. Cells remaining in the upper chamber were removed by cotton swab. The number of stained cells from five randomly captured fields (200×, 100× or 20×) of each insert was counted.

***In vivo* tumorigenic assay—**All animal procedures were approved by the Committee on the Use of Live Animals in Teaching and Research at the University of Hong Kong. MCF7 cells ($5\times10^6$) stably expressing *AKTIP* shRNA or vector were suspended in PBS and mixed with Matrigel in a 1:1 ratio prior to subcutaneous implantation into the 6-week-old female athymic nude mice (n = 10 per group) (Charles River Lab, Stone Ridge, NY). Two μg of 17β-estradiol valerate (APExBIO, Houston, TX) in sesame oil (Santa Cruz Biotechnology, Dallas, TX) were subcutaneously injected into the mice 1 week before tumor cell injection and every 4 days throughout the experiment. Tumor-bearing mice were sacrificed after 6 weeks. Tumor nodules collected were weighted and measured. Tumor nodules were subsequently fixed and subjected to immunohistochemistry. For drug treatment experiments, tumors were allowed to grow subcutaneously for 4 weeks before treatment started. Mice (n = 5 per group) were treated with vehicles, tamoxifen (10 mg/kg in corn oil, once every 2 days, subcutaneously) and AZD1480 (20 mg/kg in 0.1% Tween 80/0.5% hydroxylpropyl-methylcellulose, daily, orally) for 3 weeks. Estradiol valerate was injected subcutaneously into these mice throughout the experiments until sacrifice.

**Drug sensitivity assay—**MCF7 cells stably expressing *AKTIP* shRNA or vector were seeded into 96-well plates in triplicate at the density of 1,000 cells per well 24 hrs before the addition of indicated pharmacological inhibitors. Fulvestrant and the JAK2 inhibitor AZD1480 were obtained from Selleckchem (Houston, TX) whereas 4-OH-Tam was obtained from APExBIO. Cells were treated with the inhibitors at serially diluted concentrations for indicated amount of time. DMSO was used as control. Cell viability was measured using resazurin.

**Western blotting—**For western blotting, cells were lysed in RIPA buffer (25 mM Tris pH 7.4, 150 mM NaCl, 0.1% SDS, 1% NP-40, 1% sodium deoxy-cholate) containing protease and phosphatase inhibitors (Thermo Fisher Scientific). Equal amounts of proteins were separated by SDS-polyacrylamide gel electrophoresis and subsequently transferred onto PVDF membranes (GE Healthcare Life Sciences, Little Chalfont, UK). Membranes were then incubated with indicated primary antibodies overnight at 4°C and corresponding horseradish peroxidase (HRP)-linked secondary antibodies. Signal was detected using a chemiluminescence detection kit (Bio-Rad, Hercules, CA). Band intensities were quantified by densitometry using ImageJ.[88] Antibodies used in this study are listed in Table S4.

**Subcellular fractionation—**Cytosolic and nuclear fractions were isolated from cell lysates by the Minute Cytoplasmic & Nuclear Extraction Kits for Cells (Invent Biotechnologies, Plymouth, MN). Briefly, cells were first lysed in the Cytoplasmic Extraction Buffer. The cytosolic fraction was obtained from the supernatant after vortex and centrifugation. The remaining pellet was resuspended in the Nuclear Extraction Buffer to extract the nuclear fraction.

**Immunoprecipitation—**Cells were lysed in IP lysis buffer (50 mM Tris, 150 mM NaCl, 0.5% NP-40, 5 mM EDTA) supplemented with protease and phosphatase inhibitors. After the lysates (1 mg) were incubated with indicated antibodies (or IgG as negative control) overnight at 4°C, the immunocomplex was pulled down by incubation with Protein A/G

PLUS-Agarose beads (Santa Cruz Biotechnology) for 4 hrs at 4°C. The beads were then washed with IP lysis buffer before the immunoprecipitated proteins were eluted from the beads using 2×Laemmli sample buffer (62.5 mM Tris-HCl pH 6.8, 25% glycerol, 2% SDS, 0.01% bromophenol blue and 5% β-mercaptoethanol).

**Reverse phase protein array (RPPA)—**RPPA was conducted as previously described by the Functional Proteomics RPPA Core Facility of the University of Texas MD Anderson Cancer Center (Houston, TX).[93] Briefly, cell lysates (2 biological replicates per condition) at the concentration of 1.5 μg/μL were denatured in 4×SDS buffer and serially diluted lysates were printed onto nitrocellulose-coated slides. The slides were then incubated with primary antibodies prior to signal visualization by HRP and DAB colorimetric reaction. After signal intensities were quantified, “SuperCurve Fitting” was used to determine the relative protein levels through a logistic regression model.[89] Data were then normalized using bidirectional median centering across samples and antibodies to account for protein loading differences.

**Immunoprecipitation-mass spectrometry (MS)—**Cell lysates of MCF7 cells overexpressing HA-tagged *AKTIP* were subjected to immunoprecipitation using anti-HA antibody or IgG control to pull down *AKTIP* binding proteins. The eluted proteins were loaded in 8% SDS-PAGE gel and stained with Coomassie blue. Protein sample preparation, liquid chromatography tandem MS (LC-MS/MS) and data analysis were performed at the Proteomics and Metabolomics Core, Centre for PanorOmic Sciences, University of Hong Kong. Gel slices were subjected to reduction by 10 mM TCEP (Thermo Fisher Scientific), alkylation by 55 mM 2-chloroacetamide (Sigma) and protein digestion by trypsin (1 ng/μL; overnight at 37°C). Tryptic peptides were sequentially extracted from the gel with 50% Acetonitrile (ACN; J.T. Baker)/5% formic acid (Thermo Fisher Scientific) and 100% ACN and were desalted using C18 StageTips. Eluted peptides were analyzed with nanoelute UHPLC coupled to Bruker timsTOF pro mass spectrometer. Raw mass spectrometry data were processed using MaxQuant 1.6.14.0[90] and were searched against the Human UniProt FASTA database (Apr 2020; 74,824 entries). Proteins with at least one unique peptide detected in sample immunoprecipitated with anti-HA antibody but were absent in sample immunoprecipitated with IgG control were considered as AKTIP-interacting proteins.

**RNA-sequencing (RNA-seq)—**Total RNA from cells (2 biological replicates per condition) were extracted using TRIzol reagent (Invitrogen). RNA-seq and subsequent data processing were performed at the Genomics and Bioinformatics Cores, Centre for PanorOmic Sciences, University of Hong Kong. The libraries were prepared using the KAPA Stranded mRNA-Seq Kit (Roche, Pleasanton, CA). Sequencing was performed on the Illumina NovaSeq 6000 system. Raw reads were processed according to the following pipeline: sequencing reads were first filtered for adapter sequence, low quality sequence and rRNA sequence. Reads with read length ≥40 bp retained were aligned to the human genome GRCh38 using STAR version 2.5.2.[91] Differentially expressed genes (DEGs) were identified using DESeq2 version 1.26.0.[92] DEGs with adjusted p-value < 5% and fold change>1.2 were subjected to Gene ontology (GO) enrichment analysis using Metascape.[94] Gene expression data were subjected to Gene Set Enrichment Analysis (GSEA) on the hallmark gene sets using GSEA version 4.0.3.[47]

**Real-time PCR—**Two μg of total RNA isolated using TRIzol reagent were reverse transcribed to cDNA using the HiScript II 1st Strand cDNA Synthesis Kit (Vazyme, Nanjing, China). Real-time PCR was performed using ChamQ SYBR Color qPCR Master Mix (Vazyme) on the CFX96 Touch Real-Time PCR Detection System (Bio-Rad). The relative mRNA level was determined using the delta-delta Ct method with *GAPDH* as the internal control. Sequences of the primers used are shown in Table S5.

**Luciferase assay—**The 3X-ERE-TATA Firefly luciferase reporter construct (3X-ERE-TATA-luc) was a gift from Donald McDonnell (Addgene plasmid #11354).[86] MCF7 cells were cultured in phenol red-free medium with 8% charcoal stripped FBS (Gibco) for 4 days prior to transfection with *AKTIP* siRNA for 48 hrs. Cells were then co-transfected with 3X-ERE-TATA-luc or pGL2 vector with pRL-TK Renilla luciferase using Lipofectamine 3000. After 24 hrs, lysates were harvested and luciferase activities were measured by the Dual-Luciferase® Reporter Assay System (Promega, Madison, WI).

**Immunohistochemistry—**Human breast tumor tissue array (BC081116d) with known ERα status was obtained from US Biomax (Derwood, MD). The sections were deparaffinized and rehydrated through graded ethanol. Antigen retrieval was performed using citrate buffer pH 6.0 prior to incubation with 3% $H_2O_2$ to reduce endogenous peroxidase activity and blocking with goat serum. The slides were then incubated with anti-AKTIP or anti-ERα antibody overnight at 4°C followed by biotin-conjugated secondary antibody (Dako, Carpinteria, CA) incubation at room temperature for 1 hr. 3,3′-diaminobenzidine (DAB, Amresco, Solon, OH) was used to detect signal from HRP. Histoscores on an arbitrary scale: 0, no immunoreactivity; 1, weak; 2, moderate; 3, intense; and 4, very intense were used to represent protein expression of AKTIP whereas histoscores of 0, no immunoreactivity; 1, weak; 2, moderate; 3, intense were used to represent protein expression of ERα. Our ERα staining scores are completely concordant with the reported ERα intensity provided by the company.

**Organoid transfection and cell viability assay—**Transfection of siRNA at final concentration of 20 nM was carried out using Lipofectamine RNAiMAX (Invitrogen). Organoids were dissociated to single cells and resuspended in complete advanced DMEM/F12 culture medium. Organoid cell suspension was then mixed with transfection complex by gentle pipetting and incubated at 37°C in 5% $CO_2$ overnight. The next day, transfected organoids were collected, resuspended in BME, plated onto culture plates and maintained as described until harvest. Y-27632 was included in culture medium for first two days of culture to promote cell recovery. For Western blot analysis, intact organoids were harvested from domes using Cultrex Organoid Harvesting Solution (R&D systems). For cell viability assay, BME-cell suspension was seeded onto 48-well plate at a density of 2,000 cells per 10 μL BME dome for each well. For drug sensitivity assay, transfected organoids were allowed to grow for 6 days after cell seeding prior to drug or vehicle treatment for another 5 days. To determine organoid viability, CellTiter-Glo® 3D cell viability assay (Promega) was performed according to manufacturer's protocols.

**Immunofluorescence staining of organoids—**Nine days after siRNA transfection, organoids in domes were treated with 4% paraformaldehyde for 30 min on ice for fixation and harvesting. Collected organoids were washed in PBS prior to resuspension in 0.2% Triton X-100 in PBS for permeabilization for 30 min and then 3% BSA in PBS to block non-specific binding. Then, the organoids were incubated in antibody buffer (2% BSA in PBS) with primary antibodies overnight. After incubation with secondary antibodies for 3 hrs in dark, organoids in suspension were washed and resuspended in 50 μL PBS. Organoid suspension was then transferred onto glass slide evenly. After organoids were settled, excess PBS was aspirated without disturbing the samples. Slides were mounted with coverslip in the mounting medium containing DAPI. Images were captured with UltraVIEW VoX spinning disc confocal microscope (PerkinElmer, Waltham, MA).

**Patient survival analysis—**Kaplan–Meier (KM) survival analysis was performed using KM Plotter online database (https://kmplot.com/) [25] or data obtained from METABRIC.[26] Patients were dichotomized as high or low *AKTIP* mRNA levels (detected by probe 223894_s_at). The TCGA breast cancer dataset was downloaded from the Broad GDAC Firehose (http://gdac.broadinstitute.org/). *AKTIP* copy number was used for stratification of these samples. Statistical significance between groups was evaluated using logrank test.

### QUANTIFICATION AND STATISTICAL ANALYSIS

All experiments were performed three times except omics profiling (two biological replicates performed in one experiment) and immunohistochemical staining of patient tumor tissues (65 unique tissues stained once in one experiment). Data were expressed as means ± SD and analyzed by Student's *t*-test or ANOVA (unless otherwise specified) using GraphPad Prism. All p-values were two-sided and $p < 0.05$ was considered significant. Statistical details of individual experiments are indicated in the figures and corresponding figure legends.

## Supplementary Material

Refer to Web version on PubMed Central for supplementary material.

## ACKNOWLEDGMENTS

This research was supported by funding from the National Natural Science Foundation of China (grant no. 82022078) to L.W.T.C; (grant no. 81922047 and 82172596) to G.Z. and the Innovative Research Team of High-level Local Universities in Shanghai (SHSMU-ZLCX20210200) to G.Z. The authors would like to thank the RPPA Core Facility (supported by NCI grant #CA16672 and Yiling Lu's NIH R50 grant #R50CA221675) of the MD Anderson Cancer Center (Houston, TX, USA). The authors acknowledge the assistance of the University of Hong Kong Li Ka Shing Faculty of Medicine Core Facility. The publication fee is partially covered by the HKU Libraries Open Access Author Fund.

## REFERENCES

1. Chia SK, Bramwell VH, Tu D, Shepherd LE, Jiang S, Vickery T, Mardis E, Leung S, Ung K, Pritchard KI, et al. (2012). A 50-gene intrinsic subtype classifier for prognosis and prediction of benefit from adjuvant tamoxifen. Clin. Cancer Res. 18, 4465–4472. 10.1158/1078-0432.CCR-12-0286. [PubMed: 22711706]

2. Russnes HG, Lingjærde OC, Børresen-Dale AL, and Caldas C (2017). Breast cancer molecular stratification: from intrinsic subtypes to integrative clusters. Am. J. Pathol. 187, 2152–2162. 10.1016/j.ajpath.2017.04.022. [PubMed: 28733194]

3. Ellis MJ, and Perou CM (2013). The genomic landscape of breast cancer as a therapeutic roadmap. Cancer Discov. 3, 27–34. 10.1158/2159-8290.CD-12-0462. [PubMed: 23319768]

4. Cancer Genome Atlas Network (2012). Comprehensive molecular portraits of human breast tumours. Nature 490, 61–70. 10.1038/nature11412. [PubMed: 23000897]

5. Chin K, DeVries S, Fridlyand J, Spellman PT, Roydasgupta R, Kuo WL, Lapuk A, Neve RM, Qian Z, Ryder T, et al. (2006). Genomic and transcriptional aberrations linked to breast cancer pathophysiologies. Cancer Cell 10, 529–541. 10.1016/j.ccr.2006.10.009. [PubMed: 17157792]

6. Jönsson G, Staaf J, Vallon-Christersson J, Ringnér M, Holm K, Hegardt C, Gunnarsson H, Fagerholm R, Strand C, Agnarsson BA, et al. (2010). Genomic subtypes of breast cancer identified by array-comparative genomic hybridization display distinct molecular and clinical characteristics. Breast Cancer Res. 12, R42. 10.1186/bcr2596. [PubMed: 20576095]

7. Fang M, Toher J, Morgan M, Davison J, Tannenbaum S, and Claffey K (2011). Genomic differences between estrogen receptor (ER)-positive and ER-negative human breast carcinoma identified by single nucleotide polymorphism array comparative genome hybridization analysis. Cancer 117, 2024–2034. 10.1002/cncr.25770. [PubMed: 21523713]

8. Claudio PP, Howard CM, Baldi A, De Luca A, Fu Y, Condorelli G, Sun Y, Colburn N, Calabretta B, and Giordano A (1994). p130/pRb2 has growth suppressive properties similar to yet distinctive from those of retinoblastoma family members pRb and p107. Cancer Res. 54, 5556–5560. [PubMed: 7923196]

9. Helmbold H, Kömm N, Deppert W, and Bohn W (2009). Rb2/p130 is the dominating pocket protein in the p53-p21 DNA damage response pathway leading to senescence. Oncogene 28, 3456–3467. 10.1038/onc.2009.222. [PubMed: 19648966]

10. Lin YW, Yan MD, Shih YL, and Hsieh CB (2009). The basal body gene, RPGRIP1L, is a candidate tumour suppressor gene in human hepatocellular carcinoma. Eur. J. Cancer 45, 2041–2049. 10.1016/j.ejca.2009.04.012. [PubMed: 19410446]

11. Sørlie T, Perou CM, Tibshirani R, Aas T, Geisler S, Johnsen H, Hastie T, Eisen MB, van de Rijn M, Jeffrey SS, et al. (2001). Gene expression patterns of breast carcinomas distinguish tumor subclasses with clinical implications. Proc. Natl. Acad. Sci. USA 98, 10869–10874. 10.1073/pnas.191367098. [PubMed: 11553815]

12. Cheang MCU, Chia SK, Voduc D, Gao D, Leung S, Snider J, Watson M, Davies S, Bernard PS, Parker JS, et al. (2009). Ki67 index, HER2 status, and prognosis of patients with luminal B breast cancer. J. Natl. Cancer Inst. 101, 736–750. 10.1093/jnci/djp082. [PubMed: 19436038]

13. Early Breast Cancer Trialists' Collaborative Group EBCTCG; Davies C, Godwin J, Gray R, Clarke M, Cutter D, Darby S, McGale P, Pan HC, Taylor C, et al. (2011). Relevance of breast cancer hormone receptors and other factors to the efficacy of adjuvant tamoxifen: patient-level meta-analysis of randomised trials. Lancet 378, 771–784. 10.1016/S0140-6736(11)60993-8. [PubMed: 21802721]

14. Robinson DR, Wu YM, Vats P, Su F, Lonigro RJ, Cao X, Kalyana-Sundaram S, Wang R, Ning Y, Hodges L, et al. (2013). Activating ESR1 mutations in hormone-resistant metastatic breast cancer. Nat. Genet. 45, 1446–1451. 10.1038/ng.2823. [PubMed: 24185510]

15. Toy W, Shen Y, Won H, Green B, Sakr RA, Will M, Li Z, Gala K, Fanning S, King TA, et al. (2013). ESR1 ligand-binding domain mutations in hormone-resistant breast cancer. Nat. Genet. 45, 1439–1445. 10.1038/ng.2822. [PubMed: 24185512]

16. Gutierrez MC, Detre S, Johnston S, Mohsin SK, Shou J, Allred DC, Schiff R, Osborne CK, and Dowsett M (2005). Molecular changes in tamoxifen-resistant breast cancer: relationship between estrogen receptor, HER-2, and p38 mitogen-activated protein kinase. J. Clin. Oncol. 23, 2469–2476. 10.1200/JCO.2005.01.172. [PubMed: 15753463]

17. Smith CL, Nawaz Z, and O'Malley BW (1997). Coactivator and corepressor regulation of the agonist/antagonist activity of the mixed antiestrogen, 4-hydroxytamoxifen. Mol. Endocrinol. 11, 657–666. 10.1210/mend.11.6.0009. [PubMed: 9171229]

18. Osborne CK, Bardou V, Hopp TA, Chamness GC, Hilsenbeck SG, Fuqua SAW, Wong J, Allred DC, Clark GM, and Schiff R (2003). Role of the estrogen receptor coactivator AIB1 (SRC-3) and HER-2/neu in tamoxifen resistance in breast cancer. J. Natl. Cancer Inst. 95, 353–361. 10.1093/jnci/95.5.353. [PubMed: 12618500]
19. Shou J, Massarweh S, Osborne CK, Wakeling AE, Ali S, Weiss H, and Schiff R (2004). Mechanisms of tamoxifen resistance: increased estrogen receptor-HER2/neu cross-talk in ER/HER2-positive breast cancer. J. Natl. Cancer Inst. 96, 926–935. 10.1093/jnci/djh166. [PubMed: 15199112]
20. Hanker AB, Sudhan DR, and Arteaga CL (2020). Overcoming endocrine resistance in breast cancer. Cancer Cell 37, 496–513. 10.1016/j.ccell.2020.03.009. [PubMed: 32289273]
21. Turczyk L, Kitowska K, Mieszkowska M, Mieczkowski K, Czaplinska D, Piasecka D, Kordek R, Skladanowski AC, Potemski P, Romanska HM, and Sadej R (2017). FGFR2-Driven signaling counteracts tamoxifen effect on ERalpha-positive breast cancer cells. Neoplasia 19, 791–804. 10.1016/j.neo.2017.07.006. [PubMed: 28869838]
22. Moerkens M, Zhang Y, Wester L, van de Water B, and Meerman JHN (2014). Epidermal growth factor receptor signalling in human breast cancer cells operates parallel to estrogen receptor alpha signalling and results in tamoxifen insensitive proliferation. BMC Cancer 14, 283. 10.1186/1471-2407-14-283. [PubMed: 24758408]
23. Achinger-Kawecka J, Valdes-Mora F, Luu PL, Giles KA, Caldon CE, Qu W, Nair S, Soto S, Locke WJ, Yeo-Teh NS, et al. (2020). Epigenetic reprogramming at estrogen-receptor binding sites alters 3D chromatin landscape in endocrine-resistant breast cancer. Nat. Commun. 11, 320. 10.1038/s41467-019-14098-x. [PubMed: 31949157]
24. Yang J, Wei X, Tufan T, Kuscu C, Unlu H, Farooq S, Demirtas E, Paschal BM, and Adli M (2018). Recurrent mutations at estrogen receptor binding sites alter chromatin topology and distal gene expression in breast cancer. Genome Biol. 19, 190. 10.1186/s13059-018-1572-4. [PubMed: 30404658]
25. Lánczky A, and Győrffy B (2021). Web-based survival analysis tool tailored for medical research (KMplot): development and implementation. J. Med. Internet Res. 23, e27633. 10.2196/27633. [PubMed: 34309564]
26. Curtis C, Shah SP, Chin SF, Turashvili G, Rueda OM, Dunning MJ, Speed D, Lynch AG, Samarajiwa S, Yuan Y, et al. (2012). The genomic and transcriptomic architecture of 2, 000 breast tumours reveals novel subgroups. Nature 486, 346–352. 10.1038/nature10983. [PubMed: 22522925]
27. Remy I, and Michnick SW (2004). Regulation of apoptosis by the Ft1 protein, a new modulator of protein kinase B/Akt. Mol. Cell Biol. 24, 1493–1504. 10.1128/MCB.24.4.1493-1504.2004. [PubMed: 14749367]
28. Xu L, Sowa ME, Chen J, Li X, Gygi SP, and Harper JW (2008). An FTS/Hook/p107(FHIP) complex interacts with and promotes endosomal clustering by the homotypic vacuolar protein sorting complex. Mol. Biol. Cell 19, 5059–5071. 10.1091/mbc.E08-05-0473. [PubMed: 18799622]
29. Anbalagan M, and Rowan BG (2015). Estrogen receptor alpha phosphorylation and its functional impact in human breast cancer. Mol. Cell. Endocrinol. 418 Pt 3, 264–272. 10.1016/j.mce.2015.01.016. [PubMed: 25597633]
30. Lannigan DA (2003). Estrogen receptor phosphorylation. Steroids 68, 1–9. 10.1016/s0039-128x(02)00110-1. [PubMed: 12475718]
31. Zhou Y, and Liu X (2020). The role of estrogen receptor beta in breast cancer. Biomark. Res. 8, 39. 10.1186/s40364-020-00223-2. [PubMed: 32944243]
32. Sheng Y, Hong JH, Doherty R, Srikumar T, Shloush J, Avvakumov GV, Walker JR, Xue S, Neculai D, Wan JW, et al. (2012).A human ubiquitin conjugating enzyme (E2)-HECTE3ligase structure-function screen. Mol. Cell. Proteomics 11, 329–341. 10.1074/mcp.O111.013706. [PubMed: 22496338]
33. Li L, Liao J, Ruland J, Mak TW, and Cohen SN (2001). A TSG101/MDM2 regulatory loop modulates MDM2 degradation and MDM2/p53 feedback control. Proc. Natl. Acad. Sci. USA 98, 1619–1624. 10.1073/pnas.98.4.1619. [PubMed: 11172000]

34. Andersen PL, Zhou H, Pastushok L, Moraes T, McKenna S, Ziola B, Ellison MJ, Dixit VM, and Xiao W (2005). Distinct regulation of Ubc13 functions by the two ubiquitin-conjugating enzyme variants Mms2 and Uev1A. J. Cell Biol. 170, 745–755. 10.1083/jcb.200502113. [PubMed: 16129784]
35. Szklarczyk D, Gable AL, Lyon D, Junge A, Wyder S, Huerta-Cepas J, Simonovic M, Doncheva NT, Morris JH, Bork P, et al. (2019). STRING v11: protein-protein association networks with increased coverage, supporting functional discovery in genome-wide experimental datasets. Nucleic Acids Res. 47, D607–D613. 10.1093/nar/gky1131. [PubMed: 30476243]
36. Xia X, Liao Y, Huang C, Liu Y, He J, Shao Z, Jiang L, Dou QP, Liu J, and Huang H (2019). Deubiquitination and stabilization of estrogen receptor alpha by ubiquitin-specific protease 7 promotes breast tumorigenesis. Cancer Lett. 465, 118–128. 10.1016/j.canlet.2019.09.003. [PubMed: 31518603]
37. Menendez JA, and Lupu R (2017). Fatty acid synthase regulates estrogen receptor-alpha signaling in breast cancer cells. Oncogenesis 6, e299. 10.1038/oncsis.2017.4. [PubMed: 28240737]
38. Zheng J, Yang X, Harrell JM, Ryzhikov S, Shim EH, Lykke-Andersen K, Wei N, Sun H, Kobayashi R, and Zhang H (2002). CAND1 binds to unneddylated CUL1 and regulates the formation of SCF ubiquitin E3 ligase complex. Mol. Cell 10, 1519–1526. 10.1016/s1097-2765(02)00784-0. [PubMed: 12504026]
39. Sarikas A, Hartmann T, and Pan ZQ (2011). The cullin protein family. Genome Biol. 12, 220. 10.1186/gb-2011-12-4-220. [PubMed: 21554755]
40. Liu J, Furukawa M, Matsumoto T, and Xiong Y (2002). NEDD8 modification of CUL1 dissociates p120(CAND1), an inhibitor of CUL1-SKP1 binding and SCF ligases. Mol. Cell 10, 1511–1518. 10.1016/s1097-2765(02)00783-9. [PubMed: 12504025]
41. Duda DM, Borg LA, Scott DC, Hunt HW, Hammel M, and Schulman BA (2008). Structural insights into NEDD8 activation of cullin-RING ligases: conformational control of conjugation. Cell 134, 995–1006. 10.1016/j.cell.2008.07.022. [PubMed: 18805092]
42. Fan M, Bigsby RM, and Nephew KP (2003). The NEDD8 pathway is required for proteasome-mediated degradation of human estrogen receptor (ER)-alpha and essential for the antiproliferative activity of ICI 182, 780 in ERalpha-positive breast cancer cells. Mol. Endocrinol. 17, 356–365. 10.1210/me.2002-0323. [PubMed: 12554766]
43. Dhamad AE, Zhou Z, Zhou J, and Du Y (2016). Systematic proteomic identification of the heat shock proteins (hsp) that interact with estrogen receptor alpha (ERalpha) and biochemical characterization of the ERalpha-hsp70 interaction. PLoS One 11, e0160312. 10.1371/journal.pone.0160312. [PubMed: 27483141]
44. Björnström L, and Sjöberg M (2005). Mechanisms of estrogen receptor signaling: convergence of genomic and nongenomic actions on target genes. Mol. Endocrinol. 19, 833–842. 10.1210/me.2004-0486. [PubMed: 15695368]
45. Ochsner SA, Abraham D, Martin K, Ding W, McOwiti A, Kankanamge W, Wang Z, Andreano K, Hamilton RA, Chen Y, et al. (2019). The Signaling Pathways Project, an integrated 'omics knowledge-base for mammalian cellular signaling pathways. Sci. Data 6, 252. 10.1038/s41597-019-0193-4. [PubMed: 31672983]
46. Becnel LB, Ochsner SA, Darlington YF, McOwiti A, Kankanamge WH, Dehart M, Naumov A, and McKenna NJ (2017). Discovering relationships between nuclear receptor signaling pathways, genes, and tissues in Transcriptomine. Sci. Signal. 10, eaah6275. 10.1126/scisignal.aah6275. [PubMed: 28442630]
47. Subramanian A, Tamayo P, Mootha VK, Mukherjee S, Ebert BL, Gillette MA, Paulovich A, Pomeroy SL, Golub TR, Lander ES, and Mesirov JP (2005). Gene set enrichment analysis: a knowledge-based approach for interpreting genome-wide expression profiles. Proc. Natl. Acad. Sci. USA 102, 15545–15550. 10.1073/pnas.0506580102. [PubMed: 16199517]
48. Wang Y, Zhou D, Phung S, Masri S, Smith D, and Chen S (2011). SGK3 is an estrogen-inducible kinase promoting estrogen-mediated survival of breast cancer cells. Mol. Endocrinol. 25, 72–82. 10.1210/me.2010-0294. [PubMed: 21084382]
49. Wang Y, Zhou D, Phung S, Warden C, Rashid R, Chan N, and Chen S (2017). SGK3 sustains ERalpha signaling and drives acquired aromatase inhibitor resistance through maintaining

endoplasmic reticulum homeostasis. Proc. Natl. Acad. Sci. USA 114, E1500–E1508. 10.1073/pnas.1612991114. [PubMed: 28174265]

50. Gao J, Aksoy BA, Dogrusoz U, Dresdner G, Gross B, Sumer SO, Sun Y, Jacobsen A, Sinha R, Larsson E, et al. (2013). Integrative analysis of complex cancer genomics and clinical profiles using the cBioPortal. Sci. Signal. 6, pl1. 10.1126/scisignal.2004088. [PubMed: 23550210]
51. Liang H, Cheung LWT, Li J, Ju Z, Yu S, Stemke-Hale K, Dogruluk T, Lu Y, Liu X, Gu C, et al. (2012). Whole-exome sequencing combined with functional genomics reveals novel candidate driver cancer genes in endometrial cancer. Genome Res. 22, 2120–2129. 10.1101/gr.137596.112. [PubMed: 23028188]
52. Muthusami S, Prabakaran DS, Yu JR, and Park WY (2014). EGF-induced expression of Fused Toes Homolog (FTS) facilitates epithelial-mesenchymal transition and promotes cell migration in ME180 cervical cancer cells. Cancer Lett. 351, 252–259. 10.1016/j.canlet.2014.06.007. [PubMed: 24971934]
53. Cinghu S, Anandharaj A, Lee HC, Yu JR, and Park WY (2011). FTS (fused toes homolog) a novel oncoprotein involved in uterine cervical carcinogenesis and a potential diagnostic marker for cervical cancer. J. Cell. Physiol. 226, 1564–1572. 10.1002/jcp.22486. [PubMed: 20945372]
54. Katayama M, Wiklander OPB, Fritz T, Caidahl K, El-Andaloussi S, Zierath JR, and Krook A (2019). Circulating exosomal miR-20b-5p is elevated in type 2 diabetes and could impair insulin action in human skeletal muscle. Diabetes 68, 515–526. 10.2337/db18-0470. [PubMed: 30552111]
55. Muthusami S, Prabakaran DS, An Z, Yu JR, and Park WY (2013). EGCG suppresses Fused Toes Homolog protein through p53 in cervical cancer cells. Mol. Biol. Rep. 40, 5587–5596. 10.1007/s11033-013-2660-x. [PubMed: 24065519]
56. Zhu J, Zhao C, Kharman-Biz A, Zhuang T, Jonsson P, Liang N, Williams C, Lin CY, Qiao Y, Zendehdel K, et al. (2014). The atypical ubiquitin ligase RNF31 stabilizes estrogen receptor alpha and modulates estrogen-stimulated breast cancer cell proliferation. Oncogene 33, 4340–4351. 10.1038/onc.2013.573. [PubMed: 24441041]
57. Wang S, Luo H, Wang C, Sun H, Sun G, Sun N, Zeng K, Song H, Zou R, Zhou T, et al. (2017). RNF8 identified as a co-activator of estrogen receptor alpha promotes cell growth in breast cancer. Biochim. Biophys. Acta, Mol. Basis Dis. 1863, 1615–1628. 10.1016/j.bbadis.2017.02.011. [PubMed: 28216286]
58. Fan M, Park A, and Nephew KP (2005). CHIP (carboxyl terminus of Hsc70-interacting protein) promotes basal and geldanamycin-induced degradation of estrogen receptor-alpha. Mol. Endocrinol. 19, 2901–2914. 10.1210/me.2005-0111. [PubMed: 16037132]
59. Duong V, Boulle N, Daujat S, Chauvet J, Bonnet S, Neel H, and Cavaillès V (2007). Differential regulation of estrogen receptor alpha turnover and transactivation by Mdm2 and stress-inducing agents. Cancer Res. 67, 5513–5521. 10.1158/0008-5472.CAN-07-0967. [PubMed: 17545634]
60. Eakin CM, Maccoss MJ, Finney GL, and Klevit RE (2007). Estrogen receptor alpha is a putative substrate for the BRCA1 ubiquitin ligase. Proc. Natl. Acad. Sci. USA 104, 5794–5799. 10.1073/pnas.0610887104. [PubMed: 17392432]
61. Bhatt S, Xiao Z, Meng Z, and Katzenellenbogen BS (2012). Phosphorylation by p38 mitogen-activated protein kinase promotes estrogen receptor alpha turnover and functional activity via the SCF(Skp2) proteasomal complex. Mol. Cell Biol. 32, 1928–1943. 10.1128/MCB.06561-11. [PubMed: 22431515]
62. Sun J, Zhou W, Kaliappan K, Nawaz Z, and Slingerland JM (2012). ERalpha phosphorylation at Y537 by Src triggers E6-AP-ERalpha binding, ERalpha ubiquitylation, promoter occupancy, and target gene expression. Mol. Endocrinol. 26, 1567–1577. 10.1210/me.2012-1140. [PubMed: 22865929]
63. Iizuka M, Susa T, Tamamori-Adachi M, Okinaga H, and Okazaki T (2017). Intrinsic ubiquitin E3 ligase activity of histone acetyltransferase Hbo1 for estrogen receptor alpha. Proc. Jpn. Acad. Ser. B Phys. Biol. Sci. 93, 498–510. 10.2183/pjab.93.030.
64. Deshaies RJ, and Joazeiro CAP (2009). RING domain E3 ubiquitin ligases. Annu. Rev. Biochem. 78, 399–434. 10.1146/annurev.biochem.78.101807.093809. [PubMed: 19489725]
65. Goldenberg SJ, Cascio TC, Shumway SD, Garbutt KC, Liu J, Xiong Y, and Zheng N (2004). Structure of the Cand1-Cul1-Roc1 complex reveals regulatory mechanisms for the assembly of the

multisubunit cullin-dependent ubiquitin ligases. Cell 119, 517–528. 10.1016/j.cell.2004.10.019. [PubMed: 15537541]

66. Schmidt MW, McQuary PR, Wee S, Hofmann K, and Wolf DA (2009). F-box-directed CRL complex assembly and regulation by the CSN and CAND1. Mol. Cell 35, 586–597. 10.1016/j.molcel.2009.07.024. [PubMed: 19748355]
67. Pierce NW, Lee JE, Liu X, Sweredoski MJ, Graham RLJ, Larimore EA, Rome M, Zheng N, Clurman BE, Hess S, et al. (2013). Cand1 promotes assembly of new SCF complexes through dynamic exchange of F box proteins. Cell 153, 206–215. 10.1016/j.cell.2013.02.024. [PubMed: 23453757]
68. Byun B, and Jung Y (2008). Repression of transcriptional activity of estrogen receptor alpha by a Cullin3/SPOP ubiquitin E3 ligase complex. Mol. Cells 25, 289–293. [PubMed: 18414007]
69. Bröcker C, Engelbrecht-Vandré S, and Ungermann C (2010). Multisubunit tethering complexes and their role in membrane fusion. Curr. Biol. 20, R943–R952. 10.1016/j.cub.2010.09.015. [PubMed: 21056839]
70. Merigliano C, Burla R, La Torre M, Del Giudice S, Teo H, Liew CW, Chojnowski A, Goh WI, Olmos Y, Maccaroni K, et al. (2021). *AKTIP* interacts with ESCRT I and is needed for the recruitment of ESCRT III subunits to the midbody. PLoS Genet. 17, e1009757. 10.1371/journal.pgen.1009757. [PubMed: 34449766]
71. Henne WM, Buchkovich NJ, and Emr SD (2011). The ESCRT pathway. Dev. Cell 21, 77–91. 10.1016/j.devcel.2011.05.015. [PubMed: 21763610]
72. Lin WH, Dai WG, Xu XD, Yu QH, Zhang B, Li J, and Li HP (2019). Downregulation of DPF3 promotes the proliferation and motility of breast cancer cells through activating JAK2/STAT3 signaling. Biochem. Biophys. Res. Commun. 514, 639–644. 10.1016/j.bbrc.2019.04.170. [PubMed: 31076105]
73. Chang R, Song L, Xu Y, Wu Y, Dai C, Wang X, Sun X, Hou Y, Li W, Zhan X, and Zhan L (2018). Loss of Wwox drives metastasis in triple-negative breast cancer by JAK2/STAT3 axis. Nat. Commun. 9, 3486. 10.1038/s41467-018-05852-8. [PubMed: 30154439]
74. Tawara K, Scott H, Emathinger J, Ide A, Fox R, Greiner D, LaJoie D, Hedeen D, Nandakumar M, Oler AJ, et al. (2019). Co-expression of VEGF and IL-6 family cytokines is associated with decreased survival in HER2 negative breast cancer patients: subtype-specific IL-6 family cytokine-mediated VEGF secretion. Transl. Oncol. 12, 245–255. 10.1016/j.tranon.2018.10.004. [PubMed: 30439625]
75. Yamamoto T, Matsuda T, Junicho A, Kishi H, Saatcioglu F, and Muraguchi A (2000). Cross-talk between signal transducer and activator of transcription 3 and estrogen receptor signaling. FEBS Lett. 486, 143–148. 10.1016/s0014-5793(00)02296-1. [PubMed: 11113455]
76. Wang LH, Yang XY, Mihalic K, Xiao W, Li D, and Farrar WL (2001). Activation of estrogen receptor blocks interleukin-6-inducible cell growth of human multiple myeloma involving molecular cross-talk between estrogen receptor and STAT3 mediated by co-regulator PIAS3. J. Biol. Chem. 276, 31839–31844. 10.1074/jbc.M105185200. [PubMed: 11429412]
77. Binai NA, Damert A, Carra G, Steckelbroeck S, Löwer J, Löwer R, and Wessler S (2010). Expression of estrogen receptor alpha increases leptin-induced STAT3 activity in breast cancer cells. Int. J. Cancer 127, 55–66. 10.1002/ijc.25010. [PubMed: 19876927]
78. Speirs V, Kerin MJ, Walton DS, Newton CJ, Desai SB, and Atkin SL (2000). Direct activation of oestrogen receptor-alpha by interleukin-6 in primary cultures of breast cancer epithelial cells. Br. J. Cancer 82, 1312–1316. 10.1054/bjoc.1999.1097. [PubMed: 10755407]
79. Gupta N, Grebhardt S, and Mayer D (2012). Janus kinase 2--a novel negative regulator of estrogen receptor alpha function. Cell. Signal. 24, 151–161. 10.1016/j.cellsig.2011.08.016. [PubMed: 21907792]
80. Zhu N, Zhang J, Du Y, Qin X, Miao R, Nan J, Chen X, Sun J, Zhao R, Zhang X, et al. (2020). Loss of ZIP facilitates JAK2-STAT3 activation in tamoxifen-resistant breast cancer. Proc. Natl. Acad. Sci. USA 117, 15047–15054. 10.1073/pnas.1910278117. [PubMed: 32532922]
81. DeMichele AM, Clark AS, Holmes R, Volpe M, Medrano C, Troxel A, Fox K, Domchek S, Matro J, Bradbury A, et al. (2017). Targeting inflammatory pathways: a phase 2 trial of the JAK-inhibitor ruxolitinib in combination with exemestane for aromatase inhibitor-resistant, estrogen

receptor-positive breast cancer. In San Antonio Breast Cancer Symposium (Cancer Research). 10.1158/1538-7445.SABCS16-P2-08-03.

82. Bornstein G, Ganoth D, and Hershko A (2006). Regulation of neddylation and deneddylation of cullin1 in SCFSkp2 ubiquitin ligase by F-box protein and substrate. Proc. Natl. Acad. Sci. USA 103, 11515–11520. 10.1073/pnas.0603921103. [PubMed: 16861300]
83. Chua YS, Boh BK, Ponyeam W, and Hagen T (2011). Regulation of cullin RING E3 ubiquitin ligases by CAND1 in vivo. PLoS One 6, e16071. 10.1371/journal.pone.0016071. [PubMed: 21249194]
84. Ohta T, Michel JJ, Schottelius AJ, and Xiong Y (1999). ROC1, a homolog of APC11, represents a family of cullin partners with an associated ubiquitin ligase activity. Mol. Cell 3, 535–541. 10.1016/s1097-2765(00)80482-7. [PubMed: 10230407]
85. Furukawa M, Zhang Y, McCarville J, Ohta T, and Xiong Y (2000). The CUL1C-terminal sequence and ROC1 are required for efficient nuclear accumulation, NEDD8 modification, and ubiquitin ligase activity of CUL1. Mol. Cell Biol. 20, 8185–8197. 10.1128/MCB.20.21.8185-8197.2000. [PubMed: 11027288]
86. Hall JM, and McDonnell DP (1999). The estrogen receptor beta-isoform (ERbeta) of the human estrogen receptor modulates ERalpha transcriptional activity and is a key regulator of the cellular response to estrogens and antiestrogens. Endocrinology 140, 5566–5578. 10.1210/endo.140.12.7179. [PubMed: 10579320]
87. Moffat J, Grueneberg DA, Yang X, Kim SY, Kloepfer AM, Hinkle G, Piqani B, Eisenhaure TM, Luo B, Grenier JK, et al. (2006). A lentiviral RNAi library for human and mouse genes applied to an arrayed viral high-content screen. Cell 124, 1283–1298. 10.1016/j.cell.2006.01.040. [PubMed: 16564017]
88. Schneider CA, Rasband WS, and Eliceiri KW (2012). NIH Image to ImageJ: 25 years of image analysis. Nat. Methods 9, 671–675. 10.1038/nmeth.2089. [PubMed: 22930834]
89. Hu J, He X, Baggerly KA, Coombes KR, Hennessy BTJ, and Mills GB (2007). Non-parametric quantification of protein lysate arrays. Bioinformatics 23, 1986–1994. 10.1093/bioinformatics/btm283. [PubMed: 17599930]
90. Cox J, and Mann M (2008). MaxQuant enables high peptide identification rates, individualized p.p.b.-range mass accuracies and proteome-wide protein quantification. Nat. Biotechnol. 26, 1367–1372. 10.1038/nbt.1511. [PubMed: 19029910]
91. Dobin A, Davis CA, Schlesinger F, Drenkow J, Zaleski C, Jha S, Batut P, Chaisson M, and Gingeras TR (2013). STAR: ultrafast universal RNA-seq aligner. Bioinformatics 29, 15–21. 10.1093/bioinformatics/bts635. [PubMed: 23104886]
92. Love MI, Huber W, and Anders S (2014). Moderated estimation of fold change and dispersion for RNA-seq data with DESeq2. Genome Biol. 15, 550. 10.1186/s13059-014-0550-8. [PubMed: 25516281]
93. Tibes R, Qiu Y, Lu Y, Hennessy B, Andreeff M, Mills GB, and Kornblau SM (2006). Reverse phase protein array: validation of a novel proteomic technology and utility for analysis of primary leukemia specimens and hematopoietic stem cells. Mol. Cancer Ther. 5, 2512–2521. 10.1158/1535-7163.MCT-06-0334. [PubMed: 17041095]
94. Zhou Y, Zhou B, Pache L, Chang M, Khodabakhshi AH, Tanaseichuk O, Benner C, and Chanda SK (2019). Metascape provides a biologist-oriented resource for the analysis of systems-level datasets. Nat. Commun. 10, 1523. 10.1038/s41467-019-09234-6. [PubMed: 30944313]

## Highlights

- *AKTIP* loss selectively promotes tumorigenesis of ERα-positive breast cancer cells
- *AKTIP* loss leads to ERα protein stabilization and JAK2/STAT3 activation
- Cullin 2-mediated ERα degradation is inhibited in *AKTIP*-depleted cells via CAND1
- *AKTIP* loss-induced endocrine resistance can be overcome by inhibiting JAK2/STAT3

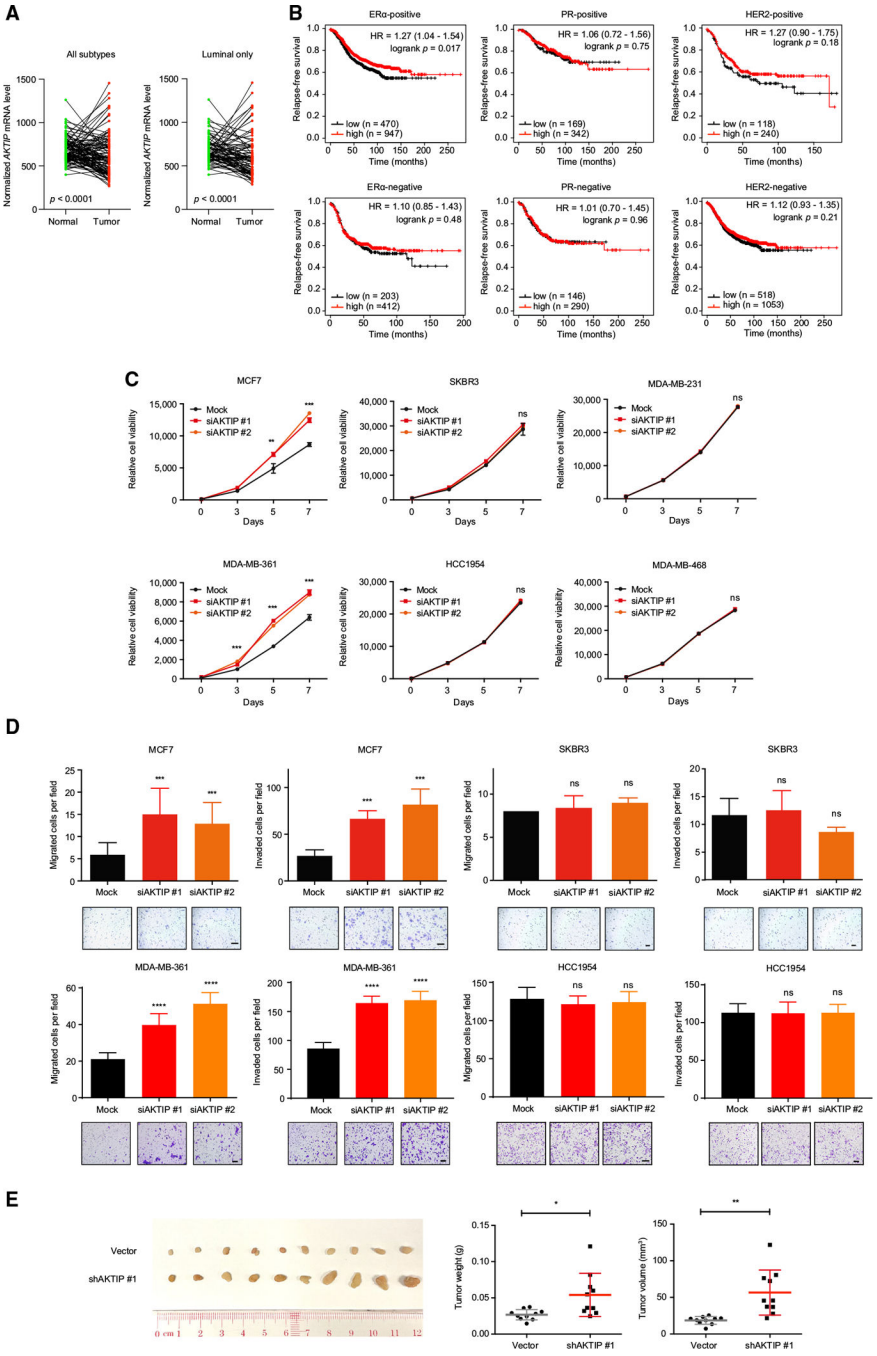


**Figure 1. *AKTIP* loss promotes tumorigenic phenotypes selectively in luminal breast cancer cells**

(A) *AKTIP* mRNA levels between matched normal breast tissues and tumor samples of all subtypes (n = 111 pairs) or luminal subtype only (n = 84 pairs) in TCGA cohort. p values of Wilcoxon signed rank test are shown.

(B) Relapse-free survival of patients with ERα-, progesterone receptor (PR)-, and HER2-positive (top) and ERα-, PR-, and HER2-negative (bottom) breast cancer with a lower tertile of *AKTIP* mRNA level as cutoff. The analysis was generated by KM plotter using

expression data obtained from Gene Expression Omnibus datasets. Hazard ratio (HR), 95% confidence interval, and log rank p values are shown.

(C and D) Cells were transfected with *AKTIP* siRNA for 24 h before seeding into 96-well plate or culture insert.

(C) Cell viability of ERα-positive MCF7 and MDA-MB-361 cells (left), HER2-enriched SKBR3 and HCC1954 cells (middle), and basal-like MDA-MB-231 and MDA-MB-468 cells (right) was measured over 7 days. Day 0 was the day of cell seeding. Data show mean ± SD of triplicates and one representative of three independent experiments. **p < 0.01; ***p < 0.001; ns, no significant difference by two-way ANOVA with Sidak's multiple comparison test.

(D) Cells were allowed to migrate or invade for 16 h. Mean numbers (top) and representative images (bottom) of migrated or invaded MCF7, MDA-MB-361, SKBR3, or HCC1954 cells of five fields at a magnification of 100× (MCF7 and HCC1954), 200× (MDA-MB-361), or 20× (SKBR3) are shown. Scale bar, 200 μm. Data shown are one of three independent experiments.

(E) MCF7 cells stably expressing *AKTIP* shRNA or vector were subcutaneously injected into nude mice (n = 10) for 6 weeks. Image of tumor nodules extracted (left) and tumor weight and volume (right) are shown. Data are presented as mean ± SD. *p < 0.05; **p < 0.01; ***p < 0.001; ****p < 0.0001; ns, no significant difference compared with mock or vector using t test.

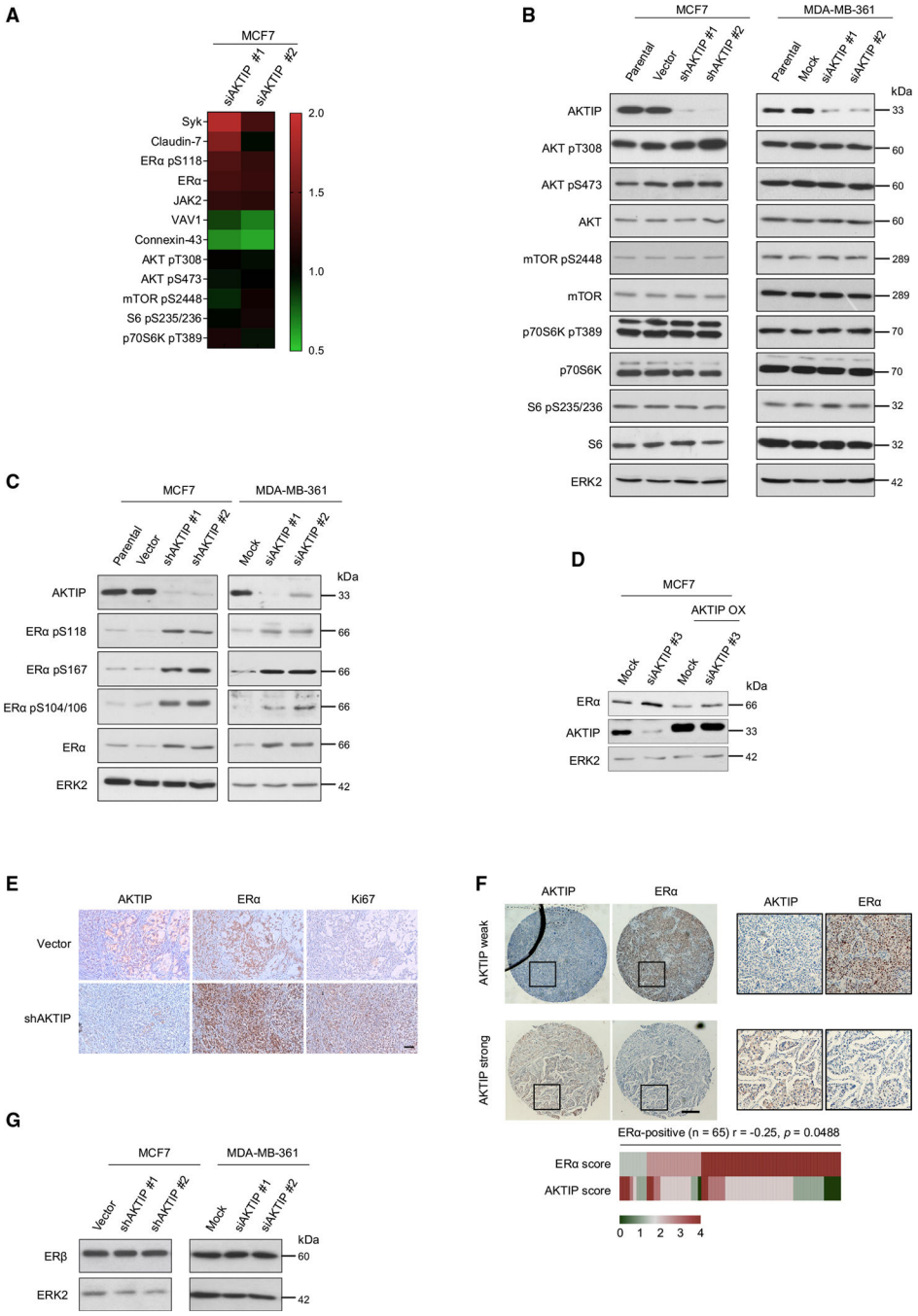


**Figure 2. ERα protein levels are increased in *AKTIP*-depleted luminal breast cancer cells**

(A) Lysates of MCF7 cells transfected with *AKTIP* siRNA or mock for 72 h were harvested for reverse-phase protein array. The heatmap shows proteins with >20% change in levels in *AKTIP*-depleted cells normalized to mock-transfected cells.

(B and C) Lysates of MCF7 cells stably expressing *AKTIP* shRNA and MDA-MB-361 cells transfected with *AKTIP* siRNA for 72 h were subjected to western blotting for proteins of the (B) AKT and (C) ERα pathways. ERK2 was loading control.

(D) Cells were transfected with siRNA targeting the 3′ UTR of *AKTIP*. Eight h later, lentivirus for *AKTIP* overexpression (OX) was added to the culture for another 72 h prior to protein harvest for western blotting. ERK2 was loading control.

(E) Representative immunohistochemical images of *AKTIP*-depleted and vector xenograft tumor sections stained with anti-*AKTIP*, anti-ERα, or anti-Ki67 antibody. Scale bar, 100 μm.

(F) Human breast tumor tissue samples were subjected to immunohistochemical staining using anti-*AKTIP* or anti-ERα antibody. Top, representative immunohistochemical images. The boxes depict magnified areas. Scale bar, 200 μm. Bottom, heatmap illustrating the correlation between ERα and *AKTIP* staining intensities. p value of Pearson correlation analysis is shown.

(G) Lysates of MCF7 cells stably expressing *AKTIP* shRNA and MDA-MB-361 cells transfected with *AKTIP* siRNA for 72 h were subjected to western blotting for ERβ levels. The western blots shown are representatives of three independent experiments.

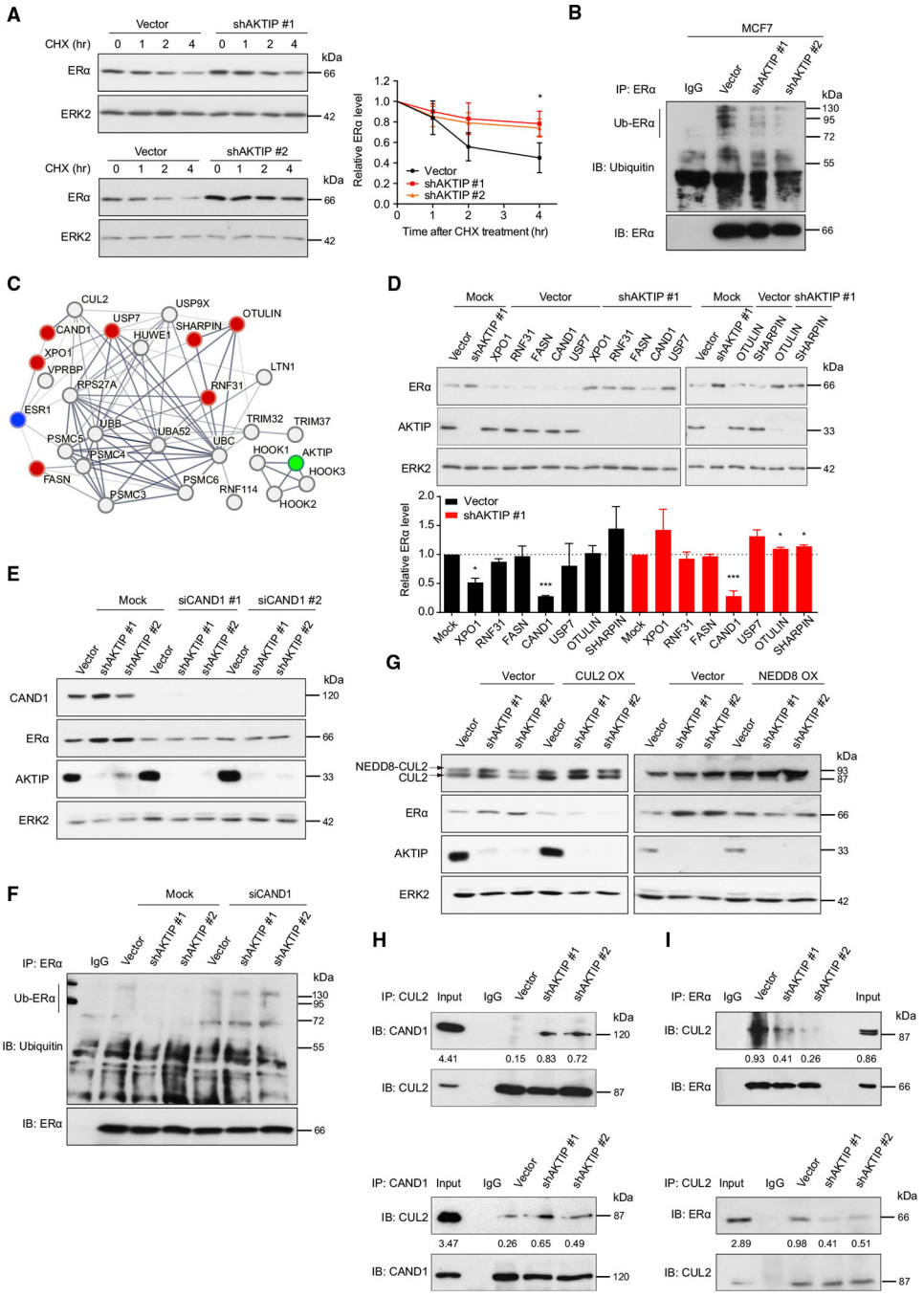


**Figure 3. Protein stability of ERα is enhanced in cells with *AKTIP* loss through CAND1**

(A) MCF7 cells stably expressing *AKTIP* shRNA or vector were treated with 10 μg/mL cycloheximide (CHX) for the indicated hours before being subjected to western blotting. ERK2 was loading control. The graph shows band intensities quantified by densitometry in ImageJ and normalized to that at 0 h (n = 3). *p < 0.05 using two-way ANOVA for comparison between groups with Sidak's multiple comparison test.

(B) Lysates of *AKTIP*-depleted or vector control cells were subjected to immunoprecipitation (IP) with anti-ERα antibody before western blotting (immunoblotting

[IB]). ERα protein levels were normalized prior to IP by using proportionally different amounts of lysates. IP with normal immunoglobulin G (IgG) was control.

(C) AKTIP-bound proteins pulled down in MCF7 cells were identified by mass spectrometry. Protein interaction network of the protein partners was generated by STRING. ERα, which was not pulled down in the IP, was included in the STRING analysis to reveal proteins that potentially interact with ERα. Only proteins in the ubiquitin/proteasome degradation pathway are shown in the network map. Red dots: hits known to inhibit protein ubiquitination. Line thickness reflects the degree of confidence of the interaction.

(D–G) MCF7 cells stably expressing *AKTIP* shRNA or vector were transfected with (D) a pool of 4 siRNA of each gene indicated, (E and F) individual siRNA of *CAND1*, or (G) OX plasmid of *CUL2* or *NEDD8* for 72 h. Protein lysates were harvested for western blotting or IP.

(H) Lysates of *AKTIP*-depleted or vector control cells were subjected to IP with anti-CUL2 antibody (top) or anti-CAND1 antibody (bottom) using equal amounts of lysates.

(I) Lysates of *AKTIP*-depleted or vector control cells were subjected to IP with anti-ERα antibody using proportionally different amounts of lysates for equal ERα levels (top) or anti-CUL2 antibody using equal amounts of lysates (bottom). IP with IgG was control. Input was lysate without the IP procedure. Relative densitometric values (after normalization with the immunoprecipitated proteins) are provided below the blots. *$p < 0.05$; ***$p < 0.001$; ns, no significant difference compared with mock using t test ($n = 3$). The western blots shown are representatives of three independent experiments.

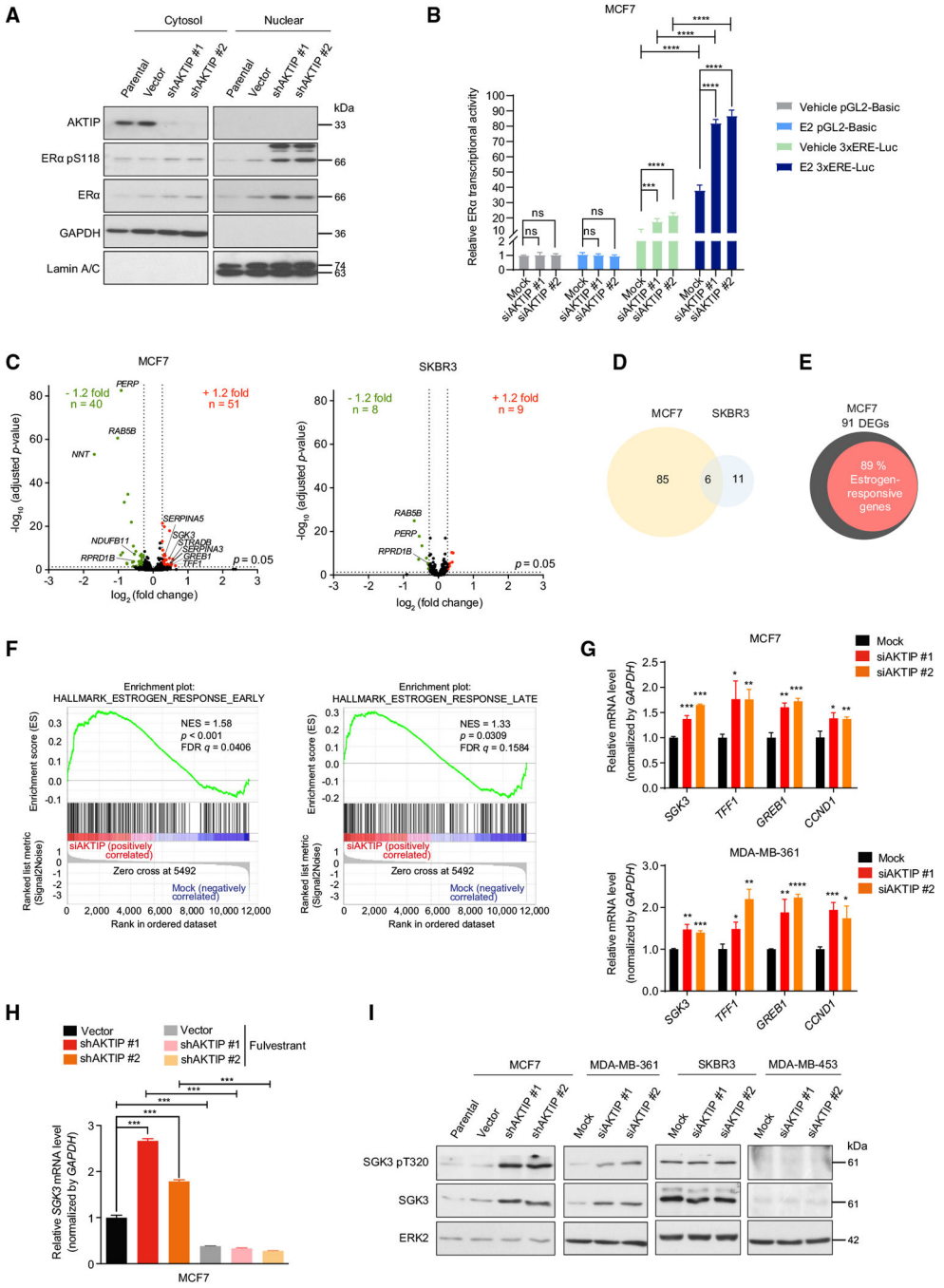


**Figure 4. MCF7 cells with *AKTIP* loss exhibit ERα-responsive gene expression profiles**

(A) Lysates of MCF7 cells stably expressing *AKTIP* shRNA or vector were harvested for subcellular fractionation before western blotting. GAPDH and lamin A/C are markers for the cytosolic and nuclear fractions, respectively.

(B) MCF7 cells were transfected with *AKTIP* siRNA for 48 h prior to co-transfection of pRL-TK Renilla luciferase plasmids and 3x-ERE-TATA firefly luciferase or pGL2-Basic (vector backbone without 3x-ERE-TATA) plasmids. Cells were treated with or without

10 nM estradiol (E2) for 24 h. Dual-luciferase reporter assay was performed, and the normalized firefly/Renilla luciferase activities are presented.

(C) Volcano plots showing the distribution of DEGs (adjusted p < 5%, fold change > 1.2) identified from the RNA-seq analysis of MCF7 (left) and SKBR3 (right) cellsupon *AKTIP* loss (n = 2). Upregulated and downregulated DEGs are labeled in red and green, respectively. Labeled genes are DEGs validated by real-time PCR.

(D) Venn diagram showing the overlap of DEGs between MCF7 and SKBR3 upon *AKTIP* knockdown.

(E) Diagram showing the percentage of estrogen-responsive genes among the 91 DEGs identified in MCF7 upon *AKTIP* knockdown.

(F) GSEA analysis of hallmark gene sets representing early and late estrogen response using ranked gene expression changes in *AKTIP* siRNA-transfected cells compared with mock-transfected cells. Normalized enrichment score (NES), p value, and FDR are shown.

(G) Total RNA of MCF7 and MDA-MB-361 cells transfected with *AKTIP* siRNA for 72 h was harvested for real-time PCR. *GAPDH* was internal control.

(H) MCF7 cells stably expressing *AKTIP* shRNA or vector were treated with 10 nM fulvestrant for 48 h before total RNA was harvested for real-time PCR.

(I) Lysates of MCF7 cells stably expressing *AKTIP* shRNA, MDA-MB-361, SKBR3, and MDA-MB-453 cells transfected with *AKTIP* siRNA for 72 h were subjected to western blotting. ERK2 was loading control. Data are presented as mean ± SD. *p < 0.05; **p < 0.01; ***p < 0.001; ****p < 0.0001; ns, no significant difference using ordinary one-way ANOVA for analysis within group and two-way ANOVA for comparison between groups with Sidak's multiple comparison test. Bar graphs are mean ± SD of triplicates and one representative of three independent experiments. The western blots shown are representatives of three independent experiments.

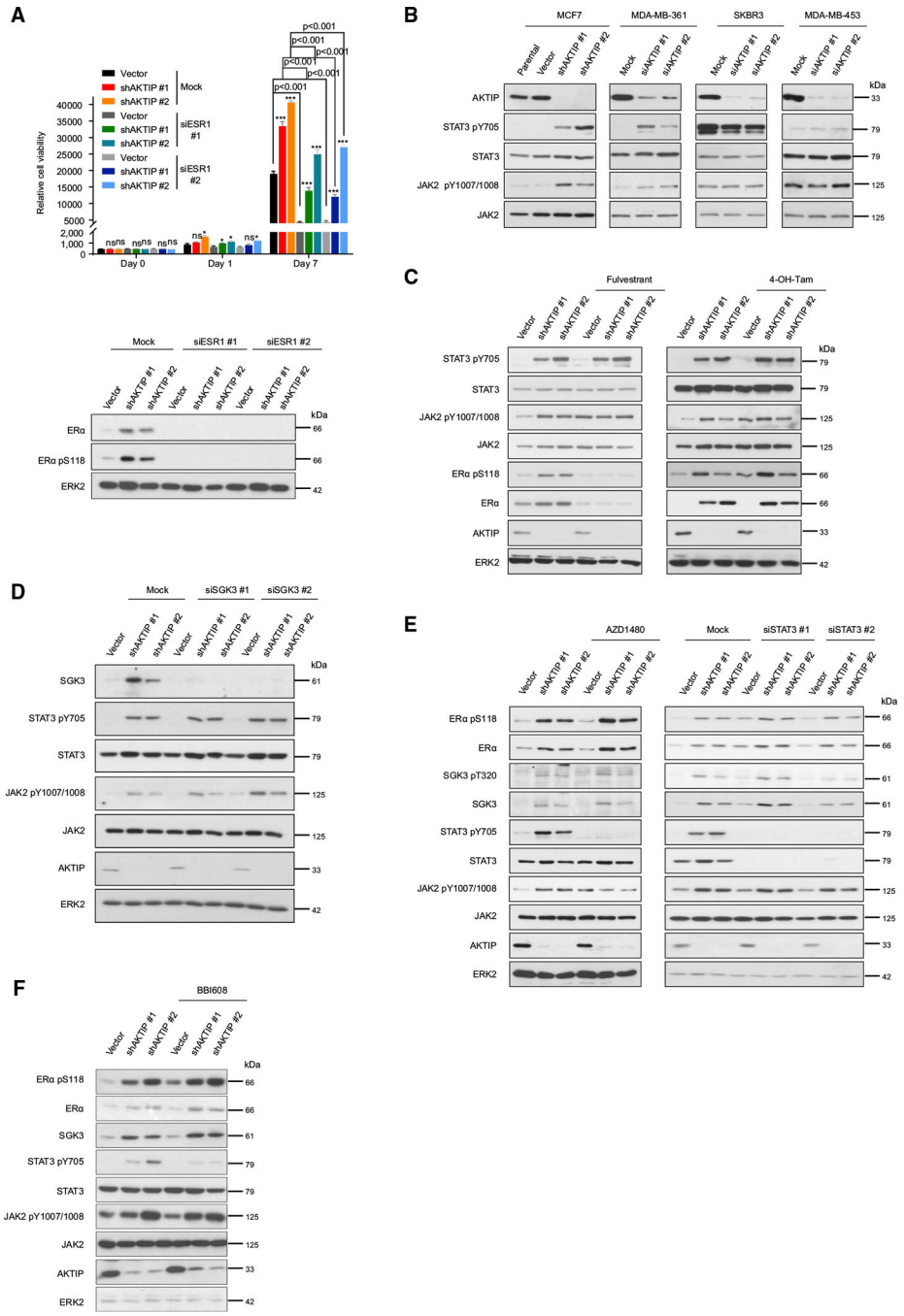


**Figure 5. Loss of *AKTIP* activates JAK2/STAT3 signaling in ERα-positive breast cancer cells**

(A) MCF7 cells stably expressing *AKTIP* shRNA or vector were transfected with *ESR1* siRNA for 24 h before cells were seeded for cell viability assay, which was measured over 7 days (top), or lysates were harvested for western blotting 8 days after siRNA transfection (bottom). ERK2 was loading control. Day 0 was the day of cell seeding. Bar graphs are mean ± SD of triplicates and one representative of three independent experiments.

(B) Lysates of MCF7 cells stably expressing *AKTIP* shRNA, MDA-MB-361, SKBR3, and MDA-MB-453 cells transfected with *AKTIP* siRNA for 72 h were subjected to western blotting.

(C–F) MCF7 stable cells were (C) treated with 10 nM fulvestrant or 1 μM 4-hydroxytamoxifen (4-OH-Tam) for 48 h; (D) *SGK3* siRNA for 72 h; (E) 2 μM AZD1480 for 24 h or *STAT3* siRNA for 72 h; or (F) 0.5 μM BBI608 for 2 h before lysates were harvested for western blotting. *$p < 0.05$; ***$p < 0.001$; ns, no significant difference compared with vector using t test. The western blots shown are representatives of three independent experiments.

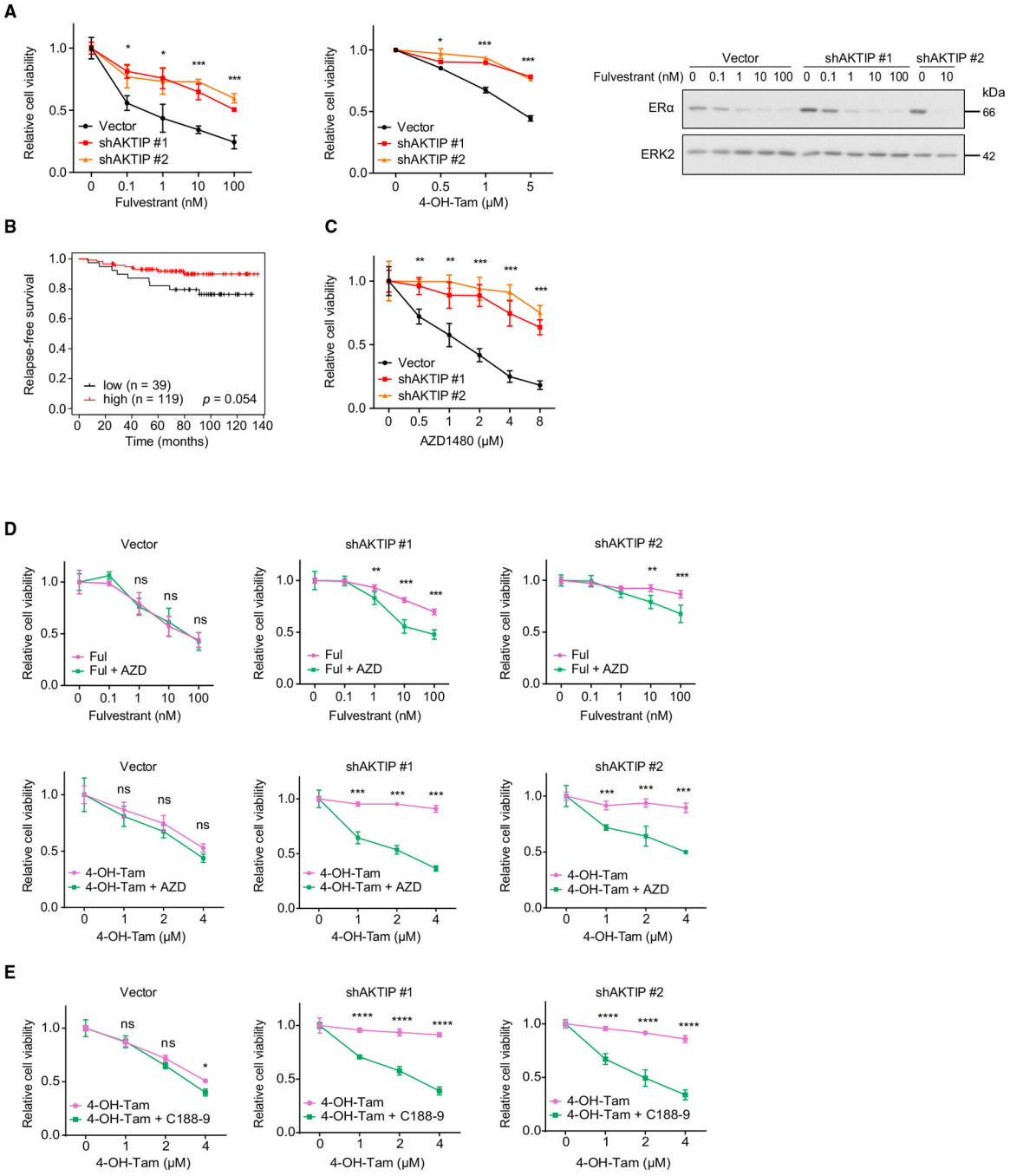


**Figure 6. JAK2 or STAT3 inhibition resensitizes *AKTIP*-depleted cells to ERα antagonists *in vitro***

(A) MCF7 cells stably expressing *AKTIP* shRNA or vector were treated with serially diluted concentrations of fulvestrant for 72 h or 4-OH-Tam for 6 days prior to cell viability assay. Lysates of cells treated with the indicated concentration of fulvestrant were harvested for western blotting (right). ERK2 was loading control.

(B) Relapse-free survival of patients with ERα-positive breast cancer with high or low *AKTIP* mRNA levels stratified at the lower quartile. Cohorts of patients with ERα-positive

breast cancer treated with adjuvant tamoxifen (n = 158) were selected for the analysis in the KM plotter. Log rank p value is shown.

(C) MCF7 cells stably expressing *AKTIP* shRNA or vector were treated with serial concentrations of AZD1480 for 72 h.

(D and E) MCF7 cells stably expressing *AKTIP* shRNA or vector were treated with serial concentrations of (D, top) fulvestrant (Ful) with or without 2 μM AZD1480 (AZD) for 72 h; (D, bottom) 4-OH-Tam with or without 2 μM AZD; or (E) 4-OH-Tam with or without 2 μM C188–9 for 6 days. The plots show mean ± SD of triplicates and one representative of three independent experiments. *p < 0.05; **p < 0.01; ***p < 0.001; ****p < 0.0001; ns, no significant difference by two-way ANOVA with Sidak's multiple comparison test.

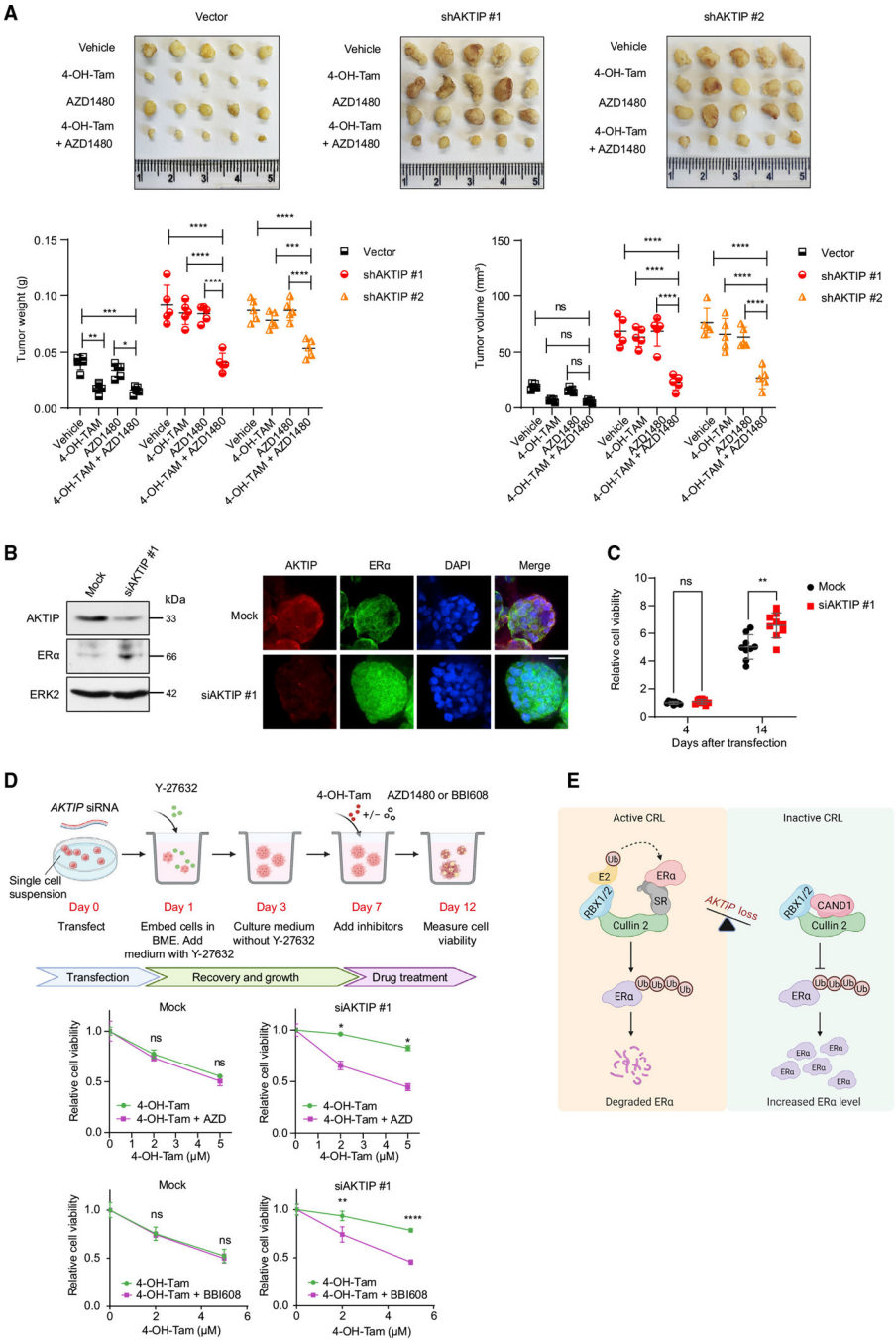


**Figure 7. Responses of *AKTIP*-depleted cells to ERα antangonist or JAK2/STAT3 inhibitor alone or in combination in xenograft and human breast cancer organoid models**

(A) Vector-expressing or *AKTIP* shRNA-expressing MCF7 tumor-bearing mice (n = 5) were treated with vehicles, 4-OH-TAM (10 mg/kg; once every 2 days), and AZD (20 mg/kg; daily) alone or in combination for 3 weeks. Images of the tumors (top) as well as graphs of tumor weight and tumor volume (bottom) are presented. Error bars represent SD. *p < 0.05; **p < 0.01; ***p < 0.001; ****p < 0.0001; ns, no significant difference using two-way ANOVA with Sidak's multiple comparison test.

(B and C) Human breast cancer organoids were transfected with *AKTIP* siRNA (B) for 9 days prior to harvest for western blotting or immunofluorescence staining or (C) for a period of 14 days, and cell viability (n = 9 of three independent experiments) was measured at 4 and 14 days post-transfection. The western blots and staining shown are representatives of three independent experiments. Scale bar, 20 μm. **p < 0.01; ns, no significant difference by t test.

(D) Top, schematic illustration of the experimental design and treatment timeline of the organoids. BME, basement membrane extract. Bottom, viability of the organoids after treatment with 4-OH-Tam in the presence or absence of 2 μM AZD or 0.5 μM BBI608 for 5 days. The plots show mean ± SD of triplicates and one representative of three independent experiments. *p < 0.05; **p < 0.01; ****p < 0.0001; ns, no significant difference by two-way ANOVA with Sidak's multiple comparison test.

(E) Proposed model of regulation of ERα protein level upon *AKTIP* loss. When *AKTIP* is depleted, the binding of CAND1 with cullin 2, and thereby the regulation on cullin 2 by CAND1, is promoted. This may alter the interaction of cullin 2 with substrate receptor (SR) that binds ERα, leading to reduced binding between cullin 2 and ERα. As a result, the ubiquitination and degradation of ERα is decreased. E2, E2 ubiquitin-conjugating enzyme; RBX, RING box protein. The figure was created with BioRender.com.

## KEY RESOURCES TABLE

| REAGENT or RESOURCE | SOURCE | IDENTIFIER |
|---|---|---|
| Antibodies | | |
| AKTIP | Proteintech | Cat# 14860-1-AP; RRID: AB_2878087 |
| AKTIP | Novus | Cat# NBP2-14278; RRID: AB_2924781 |
| AKTIP | Santa Cruz Biotechnology | Cat# sc-134343; RRID: AB_2289454 |
| ERα pS118 | Cell Signaling Technology | Cat# 2511; RRID: AB_331289 |
| ERα pS167 | Cell Signaling Technology | Cat# 5587; RRID: AB_10693297 |
| ERα pS104/106 | Cell Signaling Technology | Cat# 2517; RRID: AB_2102072 |
| ERα | Cell Signaling Technology | Cat# 8644; RRID: AB_2617128 |
| ERα | Santa Cruz Biotechnology | Cat# sc-8002; RRID: AB_627558 |
| ERβ | Invitrogen | Cat# PA1-311; RRID: AB_325597 |
| SGK3 pT320 | Cell Signaling Technology | Cat# 5642; RRID: AB_10694357 |
| SGK3 | Cell Signaling Technology | Cat# 8156; RRID: AB_10949507 |
| STAT3 pY705 | Cell Signaling Technology | Cat# 9145; RRID: AB_2491009 |
| STAT3 | Cell Signaling Technology | Cat# 4904; RRID: AB_331269 |
| JAK2 pY1007/1008 | Cell Signaling Technology | Cat# 3776; RRID: AB_2617123 |
| JAK2 | Novus | Cat# NBP2-59451; RRID: AB_2924782 |
| Ubiquitin | Abcam | Cat# ab7780; RRID: AB_306069 |
| AKT pT308 | Santa Cruz Biotechnology | Cat# sc-271966; RRID: AB_10715102 |
| AKT pS473 | Cell Signaling Technology | Cat# 9271; RRID: AB_329825 |
| AKT | Cell Signaling Technology | Cat# 4691; RRID: AB_915783 |
| mTOR pS2448 | Cell Signaling Technology | Cat# 5536; RRID: AB_10691552 |
| mTOR | Cell Signaling Technology | Cat# 2983; RRID: AB_2105622 |
| S6 pS235/236 | Cell Signaling Technology | Cat# 2211; RRID: AB_331679 |
| S6 | Cell Signaling Technology | Cat# 2317; RRID: AB_2238583 |
| p70S6K pT389 | Cell Signaling Technology | Cat# 9234; RRID: AB_2269803 |
| p70S6K | Cell Signaling Technology | Cat# 9202; RRID: AB_331676 |
| HA | BioLegend | Cat# 901502; RRID: AB_2565007 |
| CAND1 | Bethyl | Cat# A302-901A; RRID: AB_10663486 |
| Cullin-2 | Bethyl<br>Santa Cruz Biotechnology | Cat# A302-476A; RRID: AB_1944215<br>Cat# sc-166506; RRID: AB_2230072 |
| USP7 | Bethyl | Cat# A300-033A; RRID: AB_203276 |
| HOOK1 | Santa Cruz Biotechnology | Cat# sc-398233; RRID: AB_2923066 |
| FASN | Santa Cruz Biotechnology | Cat# sc-55580; RRID: AB_2231427 |
| HSPA1B | Invitrogen | Cat# PA5-28369; RRID:AB_2545845 |
| HSPA1A | Sigma-Aldrich | Cat# SAB2701085; RRID: AB_2923065 |
| α/β-Tubulin | Cell Signaling Technology | Cat# 2148; RRID: AB_2288042 |
| Lamin A/C | Cell Signaling Technology | Cat# 2032; RRID: AB_2136278 |
| GAPDH | GenScript | Cat# A00192 |
| ERK2 | Santa Cruz Biotechnology | Cat# sc-154; RRID: AB_2141292 |
| HRP-linked anti-mouse IgG secondary antibody | GE Healthcare | Cat# NA931; RRID: AB_772210 |

| REAGENT or RESOURCE | SOURCE | IDENTIFIER |
|---|---|---|
| HRP-linked anti-rabbit IgG secondary antibody | GE Healthcare | Cat# NA934; RRID: AB_772206 |
| Bacterial and virus strains | | |
| DH5α competent *E. coli* cells | Thermo Fisher Scientific | Cat#EC0112 |
| Biological samples | | |
| Human breast tumor tissue array | US Biomax | Cat# BC081116d |
| Chemicals, peptides, and recombinant proteins | | |
| Lipofectamine RNAiMAX | Invitrogen | Cat# 13778150 |
| Lipofectamine 3000 | Invitrogen | Cat# L3000015 |
| Resazurin sodium salt | Sigma-Aldrich | Cat# R7017 |
| Matrigel® Growth Factor Reduced (GFR) Basement Membrane Matrix | Corning | Cat# 354230 |
| Matrigel® Basement Membrane Matrix | Corning | Cat# 354234 |
| 17β-estradiol valerate | APExBIO | Cat# B1506 |
| Fulvestrant | Selleckchem | Cat# S1191 |
| AZD1480 | Selleckchem | Cat# S2162 |
| 4-OH-Tam | APExBIO | Cat# B6167 |
| BBI608 (Napabucasin) | MedChemExpress | Cat# HY-13919 |
| Pierce Protease Inhibitor Mini Tablets | Thermo Fisher Scientific | Cat# A32953 |
| Protein A/G PLUS-Agarose beads | Santa Cruz Biotechnology | Cat# sc-2003 |
| Cycloheximide (CHX) | Caymen Chemical | Cat# 14126 |
| TRIzol | Invitrogen | Cat# 15596018 |
| 3,3′-diaminobenzidine (DAB) | Amresco | Cat# E885 |
| Cultrex reduced growth factor basement membrane extract (type 2, Pathclear) | R&D systems | Cat# 3533-010-02 |
| B-27 supplement | Thermo Fisher Scientific | Cat# 17504044 |
| L-glutamine | Thermo Fisher Scientific | Cat# 25030081 |
| Nicotinamide | Sigma-Aldrich | Cat# N0636 |
| N-acetylcysteine | Sigma-Aldrich | Cat# A9165 |
| Noggin | PeproTech | Cat# 120-10C |
| EGF | PeproTech | Cat# AF100-15 |
| FGF-10 | PeproTech | Cat# 100-26 |
| FGF-7 | PeproTech | Cat# 100-19 |
| Neuregulin-1 | PeproTech | Cat# 100-03 |
| A83-01 | PeproTech | Cat# 9094360 |
| R-spondin-1 | PeproTech | Cat# 120-38 |
| HEPES | Thermo Fisher Scientific | Cat# 15630080 |
| SB202190 | LC Laboratories | Cat# S-1700 |
| TrypLE Express | Thermo Fisher Scientific | Cat# 12604021 |
| Y-27632 | LC Laboratories | Cat# Y-5301 |
| Cultrex Organoid Harvesting Solution | R&D systems | Cat# 3700-100-01 |

| REAGENT or RESOURCE | SOURCE | IDENTIFIER |
|---|---|---|
| Critical commercial assays | | |
| Minute Cytoplasmic & Nuclear Extraction Kits for Cells | Invent Biotechnologies | Cat# SC-003 |
| HiScript II 1st Strand cDNA Synthesis Kit | Vazyme | Cat# R211 |
| ChamQ SYBR Color qPCR Master Mix | Vazyme | Cat# Q411 |
| Dual-Luciferase® Reporter Assay System | Promega | Cat# E1910 |
| CellTiter-Glo® 3D Cell Viability Assay | Promega | Cat# G9681 |
| Deposited data | | |
| RNA-seq data for *AKTIP* siRNA- and mock-transfected MCF7 and SKBR3 cells | This paper | GEO Accession: GSE209693 |
| AKTIP IP-MS data | This paper | ProteomeXchange identifier: PXD035716 |
| Experimental models: Cell lines | | |
| Human: MCF7 | ATCC | HTB-22 |
| Human: MDA-MB-361 | ATCC | HTB-27 |
| Human: MDA-MB-175 | ATCC | HTB-25 |
| Human: BT474 | ATCC | HTB-20 |
| Human: T47D | ATCC | HTB-133 |
| Human: MDA-MB-453 | ATCC | HTB-131 |
| Human: SKBR3 | ATCC | HTB-30 |
| Human: MDA-MB-231 | ATCC | HTB-26 |
| Human: HCC1954 | ATCC | CRL-2338 |
| Human: MDA-MB-468 | ATCC | HTB-132 |
| Experimental models: Organisms/strains | | |
| Mouse: BALB/cAnN-nu (Nude) | Charles River Lab | N/A |
| Oligonucleotides | | |
| See Table S3 for list of siRNA and shRNA sequences | This paper | N/A |
| See Table S5 for list of primer sequences for real-time PCR | This paper | N/A |
| Recombinant DNA | | |
| pcDNA3-myc3-CUL2 | (Ohta et al.,1999)[84] | Addgene Plasmid #19892 |
| pcDNA3-myc3-NEDD8 | (Furukawa et al., 2000)[85] | Addgene Plasmid #19943 |
| 3X-ERE-TATA-luc | (Hall et al., 1999)[86] | Addgene Plasmid #11354 |
| pLKO.1-Puro-shAKTIP | (Moffat et al., 2006)[87] | N/A |
| pLenti6.3-Blast-HA-AKTIP | This paper | N/A |
| Software and algorithms | | |
| ImageJ | (Schneider et al., 2012)[88] | https://imagej.nih.gov/ij/ |
| SuperCurve Fitting | (Hu et al., 2007)[89] | https://bioinformatics.mdanderson.org/public-software/supercurve/ |

| REAGENT or RESOURCE | SOURCE | IDENTIFIER |
|---|---|---|
| MaxQuant v1.6.14.0 | (Cox et al., 2008)[90] | https://www.maxquant.org/ |
| STAR RNA-seq aligner v2.5.2 | (Dobin et al., 2013)[91] | https://github.com/alexdobin/STAR |
| DESeq2 v1.26.0 | (Love et al., 2014)[92] | https://bioconductor.org/packages/release/bioc/html/DESeq2.html |
| GSEA v4.0.3 | (Subramanian et al., 2005)[47] | https://www.gsea-msigdb.org/ |
| KM Plotter | (Lanczky et al., 2021)[25] | https://kmplot.com/analysis/index.php?p=service&cancer=breast |
| GraphPad Prism | GraphPad Software | https://www.graphpad.com/ |